C.P. No. 251
(17,566)
A.R.C. Technical Report

C.P. No. 251
(17,566)
A.R.C. Technical Report

MINISTRY OF SUPPLY

AERONAUTICAL RESEARCH COUNCIL

CURRENT PAPERS

ROYAL AIRCRAFT ESTABLISHMENT
LIBRARY
BEDFORD.

Preliminary Low Speed Wind Tunnel Tests on Flat Plates and Air Brakes:

Flow, Vibration and Balance Measurements

By

R. Fail, T. B. Owen and R. C. W. Eyre

LONDON: HER MAJESTY'S STATIONERY OFFICE

1956

SIX SHILLINGS NET

C.P. No. 251

U.D.C. No.533.691.152.3 : 533.6.048.3

Technical Note No. Aero.2356

January, 1955

ROYAL AIRCRAFT ESTABLISHMENT

Preliminary low speed wind tunnel tests on flat plates and air brakes: flow, vibration and balance measurements

by

R. Fail,
T.B. Owen
and
R.C.W. Eyre

SUMMARY

Flow measurements have been made behind sharp edged flat plates: (a) at 90° for various shapes, and (b) for a square plate over an incidence range. The results of (a) show a closed bubble about 3 plate sides long, with a constant pressure boundary up to the maximum diameter, followed by mixing. Measurements of velocity fluctuations were made for (b), showing that a regular shedding of turbulent eddies occurs for $\theta = 50°$ and over, but stops by 40°. Large random low frequency longitudinal fluctuations are associated with the shedding.

Lift, drag and pitching moment increments were measured on a square plate mounted on (a) a long cylinder and (b) near the end of several shapes of rear fuselage, to see how the moments on opening the brake could be modified. Velocity fluctuation measurements, at 70° only, show a much reduced longitudinal unsteadiness when the plate is in proximity to the fuselage. Comparative tests were made on a cascade brake[3] and show that no shedding occurs.

LIST OF CONTENTS

LIST OF TABLES

LIST OF ILLUSTRATIONS

LIST OF ILLUSTRATIONS (Contd)

1 Introduction

Tests are being made in low speed wind tunnels with the main object of providing data for the design of air brakes. The results are also of interest as a contribution to the knowledge of the flow behind bluff bodies.

Some preliminary measurements have been made of the drag and the nature of the flow behind isolated flat plates of various shapes over a range of incidence. Both the mean flow pattern and the longitudinal velocity fluctuations have been studied.

Lift, drag and pitching moment have been measured on a body fitted with a square flat plate brake to explore the possibility of getting no change in pitching moment over a range of brake angle. One of these brakes was used for an investigation of vibration and showed a much steadier flow due to putting the brake on the body. Further work on this is to be done.

Types of air brakes other than simple flat plates will be tested, such as slotted and perforated plates. From Australian tests, it appears that a cascade[3] may have advantages and some tests have already been made on such a brake. The results are included in the present note.

2 Experiments with isolated flat plates

2.1 Description of tests

The experiments can be divided roughly into three groups:

(1) Measurements were made of the drag, and of the mean velocities behind plates perpendicular to the wind. The shapes tested were a square, a circle, a 60° delta and a rectangle of aspect ratio 2.15. All of the plates had an area of 25 sq.in.* and the edges were chamfered at 30° as shown in Fig.1.

(2) Further drag measurements were made on plates perpendicular to the wind with aspect ratios of 5, 10 and 20, maintaining an area of 25 sq.in.

(3) Tests were made on the square plate over an incidence range from 27° to 90°. Measurements were made of the drag and of the velocity fluctuations in a plane 15.3 in. behind the plate.

All of these experiments were made in the 4 ft × 3 ft tunnel at a speed of 140 ft/sec. The plates were mounted on the upstream end of a rod about 3 ft long and 0.5 in. diameter on the axis of the tunnel. The downstream end of the rod was supported by struts attached to the tunnel walls; the rod was also supported just behind the plate by means of three wires. A sketch of the rig is given in Fig.1.

For drag measurements, a small capacity-type balance was constructed and fitted between the rod and plate as shown in Fig.1. In order to reduce the support interference with the plate at small angles, a short length of streamline rod was interposed between the rod and plate (as shown in Fig.1) when velocity traverses were being made behind the plate.

---

*Except for the rectangle which was intended to be of aspect ratio 2.0 but was made in error to have an aspect ratio of 2.15 and an area of 27 sq.ins.

Traverses behind the plates were made with pitot-static tubes and with a hot wire using the apparatus shown in Fig.1. An elliptic section tube spanned the tunnel and carried a sliding block which could be traversed from outside the tunnel. Vertical movements were obtained by means of cranked holders, and fore and aft movements were made by moving the whole traversing gear bodily. The pitot and static tubes were kept parallel to the tunnel axis. Measurements of the reverse velocities behind the centre of the plate were made with pitot-static tubes attached to the central rod but pointing downstream.

The hot wire was arranged to be normal to the free stream direction. The associated equipment which included a vibration analyser was basically that described in Refs.1 and 2.

2.2 Velocity measurements

The velocity contours shown in Fig.4 were drawn from measurements made with pitot and static tubes set parallel to the tunnel axis in planes 3 in, 6 in, 12 in. and 24 in. downstream of the plates and also 18 in. downstream in the case of the square and rectangular plates. The contours of velocity and velocity fluctuations shown in Fig.5 were drawn from measurements made with a hot wire set normal to the tunnel axis in a plane 15.3 in. downstream of the plate.

The measurements are therefore in error where the local stream direction is not parallel to the tunnel axis. For the particular pitot and static tubes used in these experiments, a check showed that the measured velocities exceeded the true velocities by 2% for 10° misalignment and 6% for 20° misalignment. It should be noted that misalignments are small near the axis of the "bubble" (see para 2.3) and near the mid-length of the bubble. The length and maximum diameter of the bubble are therefore fairly accurately determined. The hot wire measures velocity normal to its length; it is therefore substantially non directional in the plane normal to its length with a cosine effect in the plane containing its length. In the latter case the readings are therefore low by 1½% for 10° misalignment and 6% for 20° misalignment.

The measurements are also subject to errors due to the fluctuating nature of the flow[6]. In order to investigate this effect, comparative traverses have been made with hot wires and with the pitot and static tubes in a plane 18 in. behind the plate. The results which are shown in Fig.4g give some indication of the accuracy of the present measurements. Corrections have been applied to the hot wire measurements for the effect of velocity fluctuations; the discrepancy between the velocities given by normal and inclined wires suggests that these corrections are inadequate. The pitot-static measurements are uncorrected and lie above the hot wire measurements. The maximum difference between hot wire measurements and pitot-static measurements amounts to about 20% of the local velocity or 10% of the free stream velocity.

Measurements of the longitudinal velocity fluctuations were made as follows. Measurements of the mean square of the analyser output, $\overline{\left(\frac{u_A}{U}\right)^2}$, were made over a range of frequency, f. With the analyser out of circuit, measurements were made of the mean square of the total output, $\overline{\left(\frac{u}{U}\right)^2}$. The spectrum function, F(f), is defined so that F(f)df is the contribution to $\overline{\left(\frac{u}{U}\right)^2}$ of frequencies between f and f + df, i.e.

$$\left(\frac{u}{U}\right)^2 = \int_0^{\infty} F(f)\, df$$

$$= \int_{-\infty}^{+\infty} fF(f)\, d(\log f)$$

Since the analyser bandwidth ratio, ε_A, is small (= 0.10 × tuned frequency)

$$fF(f) = \left(\frac{u_A}{U}\right)^2 \Big/ \varepsilon_A \text{ approximately.}$$

By multiplying the values of $\left(\frac{u_A}{U}\right)^2$ and $\left(\frac{u}{U}\right)^2$ by $\left(\frac{U}{U_o}\right)^2$, the results are presented in terms of the free stream speed. Contours are drawn of $\frac{u}{U_o}$ and spectra are given of $fF(f), \left(= \left(\frac{u_A}{U_o}\right)^2 \Big/ \varepsilon_A\right)$ plotted against $100f/U_o$. The latter is the frequency corresponding to a free stream speed of 100 ft/sec.

The traversing gear already described was found to be unsatisfactory for holding a hot wire. The sliding block was not a good fit at all points along the elliptic tube so that a low frequency vibration of the wire may have occurred on some occasions, giving high readings of the velocity fluctuations*. A new traversing gear has been made and found satisfactory for further experiments.

Outside the velocity wake of the plate, lateral oscillations of the flow have a negligible effect on a normal wire. Obviously lateral velocity fluctuations may be important; an inclined hot wire is required to measure these components.

The present tests are therefore limited in scope and crude in character. Nevertheless some important conclusions can be drawn from them. Further experiments are being made with normal and inclined hot wires mounted on the improved traversing gear. An attempt will also be made to correlate hot wire measurements with measurements of the fluctuating pressures on an aerodynamic surface.

2.3 Results

The drag measurements** on plates at 90° gave values of the drag coefficient of 1.15 for the square plate, 1.16 for the 60° delta plate

---

*While measuring the spectra shown in Fig.6, the sliding block was temporarily fixed rigidly to the tube.

**The drags of 25 sq.inch plates in the 4' × 3' tunnel have been multiplied by a factor (1 - 0.03 C_D) for blockage, using some tests on plates of different sizes. The correction thus found is larger than was expected, and further work is being done. The correction is negligible in the 11½ ft tunnel.

and 1.13 for the circular plate. (A pressure plot of the circular plate gave a drag coefficient of 1.14).

The variation of drag with incidence for the square and delta plates is shown in Figs.2a and 2b. The square plate stalls at about $\theta = 36^\circ$, the drag coefficient falling abruptly from 0.80 to 0.60. There is a considerable hysteresis loop at the stall[4] which could not be investigated during the present tests since it was not possible to vary the incidence with wind on. The drag is reduced as the plate stalls since the reduction in induced drag is greater than the increase in profile drag. The delta plate shows a similar but less marked break in the drag curve.

The variation of drag with aspect ratio for rectangular plates at 90° is shown in Fig.3. The two-dimensional value for C_D is about 1.84 (Ref.5). The present results show that between $A = 1$ and $A = 10$, the drag coefficient increases only from 1.15 to 1.27. At values of A above 10, the drag increases more rapidly; at $A = 20$ (the highest tested) the drag coefficient was 1.47.

Velocity distributions behind the low aspect ratio plates at 90° are shown in Fig.4. It is possible to define a closed "bubble boundary" by saying that, within this boundary, the total axial flow across any section perpendicular to the axis of the plate is zero. These boundaries are shown chain dotted in Figs.4a-d. The "wake boundary", defined by saying that outside this boundary there is no loss of total head, lies outside the bubble boundary. Along the wake boundary the static pressure coefficient is constant and equal to -0.42 from the edge of the plate to about the midlength of the bubble. The corresponding velocity is $1.2\ U_0$. The mean velocity is negative near the centre of the bubble and positive near the outside; the flow is very unsteady. The pressure coefficient on the downstream face of the circular plate was found to be constant and equal to -0.42. The static pressure coefficient falls to -0.5 three inches behind the plate and to -0.6 six inches behind (Fig.4f). At twelve inches pressure recovery has begun and the coefficient is -0.35. By eighteen inches, pressure recovery is complete. At any one distance behind the plate the static pressure appears to be constant within the bubble (Fig.4e) although it varies as stated with distance from the plate, and there is a static pressure gradient between the bubble boundary and the wake boundary.

Velocity distributions in a single plane behind the square plate over a range of incidence were obtained from hot wire readings and are given on the right hand side of Fig.5. These measurements were made 15.3 in. downstream of the plate, i.e. just behind the bubble at $\theta = 90^\circ$. At $\theta = 90^\circ$ the wake is nearly circular in section with minimum velocities of about $0.3\ U_0$ in the centre. At $\theta = 60^\circ$ the wake is similar in character although distorted and displaced downwards due to the downwash behind the plate. Detailed traverses were not made at $\theta = 50^\circ$ but analysis of the velocity fluctuations at a single point (see below) suggests a flow similar to that at $\theta = 90^\circ$ and 60°. At $\theta = 40^\circ$, just above the stall, the wake is fundamentally changed. There are two separate regions of low velocity. At $\theta = 36^\circ$, just below the stall, the wake is again of this type.

Contours of velocity fluctuation are shown on the left hand side of Fig.5. There is a change from a ring of high velocity fluctuations at 90°, to a crescent shaped region at 60° (and probably 50°) and finally to two regions at 40° and 36°.

Analyses of the velocity fluctuations over the incidence range at a single point* (indicated in Fig.5) are shown in Fig.6. This point was chosen to have large velocity fluctuations over the incidence range and the hot wire was fixed rigidly to avoid vibration. The spectra are of two types. At the higher angles ($\theta = 90^\circ$, 60° and 50°) each spectrum includes a high peak value** of $fF(f)$ at a particular frequency (which varies with incidence) superimposed on a continuous spectrum. This is due to the shedding of turbulent eddies in a regular manner. At $\theta = 40^\circ$ and 36° the spectra are continuous with no peaks, and with large random fluctuations mainly at relatively high frequency. It appears that large random fluctuations at low frequency are associated with a regular shedding.

3 Experiments with a plate on a fuselage

3.1 Lift, drag and pitching moments due to plate

It has been found that a single air brake mounted behind the wing under a fuselage can, in general, only be in trim at one angle; below this angle there is a nose down moment, and above it, a nose up moment. Experiments were made to find what variables affect this behaviour.

A cylindrical body 4.5 in. diameter with faired nose was tested in the 4 ft × 3 ft tunnel:

(a) cut off with a bluff end of full diameter,

(b) with a faired tail cut off with a bluff end of 0.59 times the full diameter,

(c) with a fully faired tail.

These are called "bluff", "boat tail" and "faired tail" (Fig.7).

The pressure distributions on the bodies without brakes (Fig.13) agree until near the modified rear ends.

The brakes used were square flat plates similar to those tested alone, and could therefore only be used at fairly large angles when on the body. For most of the tests the length of the side of the brake, ℓ, was 2/3 of the body diameter. The hinge line was tangential to the body, and the gap, measured from the hinge was normally 0.2ℓ. Two further tests were made on the body with boat tail:

(a) with a larger gap (0.4ℓ)

(b) with a smaller brake ($\ell = \frac{1}{2}$ body diameter) and the normal gap.

It was found that adding the pointed tail to the boat tail does not alter the fore and aft position where the major change in pitching moment of a brake occurs (Figs.9 and 10), so it is considered more convenient to keep the same reference point for these two bodies. Brake positions are

---

*Except that the spectrum for $\theta = 90^\circ$ is an early measurement made 11.8 in. downstream and 5.0 in. from the centre line.

**The shapes (including the heights) of the peaks shown in Fig.6 are determined by the characteristics of the analyser. Strictly the results should be presented in the form of the continuous spectrum and the mean square value of the velocity fluctuation at the single frequency. For the present purpose it is sufficient to recognise the existence of peaks.

specified by giving the distance of the brake hinge from the end of the bluff or boat tail bodies and, in the case of the body with faired tail, the distance of the brake hinge from the position on the faired tail corresponding to the end of the boat tail (Fig.7).

Lift, drag and pitching moment increments due to the larger plate with gap = $\ell/5$ are given in Tables I-IV and Figs.8-10 in the form of coefficients based on the brake dimensions, the moments being about the brake hinge. These results show that if the brake is more than about 3ℓ forward of the end of the body (or the datum described above in the case of the body with faired tail) the lift and drag increments are unchanged by further forward movement. The moments at large angles are also unchanged but at small angles the moments change in a nose down direction with forward movement. As the brake is moved back, beyond the position 3ℓ forward of the end of the body, the lift increases, the drag increases to a smaller extent and the moments at large angles decrease rapidly. The details of these changes depend on the shape of the rear body.

In Figs.14-16 the moments are shown recalculated about various assumed positions of the centre of gravity, the mid position on the body with boat tail corresponding roughly to the layout of a Hunter. The second scale (of ΔC_m) which has been added to Figs.14 and 16 expresses the moment changes in terms of Hunter dimensions, taking the body diameter as the connecting variable, i.e. the model is assumed to be 1/11.67 scale. Fig.14 shows the small effects of moving the centre of gravity and varying the shape of the rear body. An analysis of the pitching moment about the centre of gravity is given in Fig.15 showing its dependence on lift. In all cases the brakes give zero trim change at an angle near 70°.

The effect of a change in gap from $\ell/5$ to $2\ell/5$ is shown by comparing Figs.9 and 11 and in Fig.16. The drag is a little less with the bigger gap and the moments are in trim at a slightly bigger brake angle (about 73°).

The effect of a smaller brake is shown by comparing Figs.9 and 12. The change in pitching moment slope as the brake approaches the end of the body agrees if the distance from the end of the body is measured in terms of the brake dimensions, and the moment coefficients of the brake about its hinge are more positive. In Fig.16 the moments are compared in terms of an assumed wing area and C.G. position and the brake angle to trim is about 66°.

The result is that a single brake under a fuselage is in balance at about 70° and gives variations in pitching moment as it is opened agreeing with those found in practice. It is not at all apparent how to vary this except by putting the brake just ahead of the centre of gravity (which means under the wing, when these results are not applicable) or by putting it near the end of the body where it can be in trim at a larger angle but has an increased variation as it is opened and closed.

3.2 Vibration

A 5 in. square plate was tested at 70° on a 7 in. diameter body in the 4 ft × 3 ft tunnel (Fig.18). The resulting spectrum is compared with that measured behind an isolated plate at 70° in Fig.17. (The latter spectrum was produced by interpolation from Fig.6). Although both spectra include peaks due to a regular shedding of turbulent eddies, the amplitude of the fluctuations is reduced by the presence of the body and the shedding frequency is increased. This suggests that the angle below which shedding does not occur may be higher when the plate is mounted on a body and further experiments will be made to investigate this.

4 Experiments with cascade brakes

4.1 Introduction

The use of a cascade as an air brake has been suggested by the Aeronautical Research Laboratory, Melbourne[3] as giving higher drag, and probably less vibration, than a flat plate. It was thought worth while to follow up this suggestion and to investigate the velocity fluctuations in the wake of a cascade.

The first cascade brake was made from an existing wind tunnel corner cascade in which the vanes were of an aerofoil section designed to leave passages of constant area between them. It was tested (with a flat plate for comparison) under the body of a Javelin model just forward of the trailing edge of the wing. Maximum drag coefficients of 1.67 for the flat plate (at 90°) and 1.82 for the cascade (at 60°) were measured. It was clear that the high drag of the flat plate was due to interference with the wing, and it seemed likely that the interference due to the cascade brake was much smaller. The cascade brake might therefore have a greater advantage in drag on a body, clear of the wing field. The tests described below were made to check this conclusion.

4.2 Description of tests

The model used in section 3 was of too small a scale for making cascade brakes conveniently, particularly as two brakes of half the flat plate area were required. A body of maximum diameter 7 in. was therefore made (Fig.18). It represents a fighter fuselage with a shortened nose. A fin was fitted but no wing or tailplane. If the model is regarded as of 1/7.5 scale, the 5 in. square flat plate represents roughly the Hunter under fuselage brake and it was fitted in a corresponding position relative to the C.G. and fin.

The brakes are also shown in Fig.18. The 5 in. square plate was used as a basis for comparison and the following cascade brakes were tested.

(a) The brake already mentioned, made from a wind tunnel corner cascade. This will be referred to as the "aerofoil cascade". The dimensions (6.54 in. × 5.75 in.) were chosen to give a reasonable number (7) of vanes and span.

The other cascade brakes, described below, were all of the sheet metal construction shown in Fig.18 and had vanes of smaller chord than the aerofoil cascade.

(b) A brake of approximately the same dimensions as the aerofoil cascade, to afford a direct comparison between the two types of construction.

(c) A brake approximately 5 in. square for direct comparison with the flat plate.

(d) A pair of brakes (on opposite sides of the body) with a total area approximately the same as the 5 in. square brake.

Measurements of the lift, drag and pitching moment increments due to these brakes over a range of angles were made in the No.1 $11\frac{1}{2}$ ft tunnel at 120 ft/sec with the body at zero incidence.

The body with the pair of sheet metal cascade brakes was then mounted in the 4 ft × 3 ft tunnel and measurements of the velocity and velocity fluctuations in a plane 15 in. downstream of the brake hinges were made with a normal hot wire. This plane corresponds roughly to the fore and aft position of the Hunter tail plane.

4.3 Results

Values of the lift, drag and pitching moment increments due to the brakes are given in lb and lb. ft at 100 ft/sec in Table V. It is considered that the various brakes are best compared by forming coefficients of lift and drag based on the gross area of each brake, S_B, i.e. the area of cut-out required to stow the brake. The results are given in this form in Fig.19. The pitching moment increments given in Fig.20 are expressed in terms of Hunter dimensions, assuming the model to be 1/7.5 scale.

Fig.19b shows that the cascade brakes produce maximum drag at about 50° compared with 90° for the flat plate. The maximum values of ΔC_{D_B} are given in the following table which also gives the values of S_B on which the coefficients are based.

Type of Brake	Width (in)	No. of vanes	Nominal length (in)	S_B (sq.ft)	θ	ΔC_{D_B}
Flat plate	5	-	5	0.174	90°	1.28
Aerofoil Cascade	5.75	7	6.54	0.304	50°	1.76
Sheet Metal Cascade	5.75	20	6.73	0.280	50°	1.41
Sheet Metal Cascade	5	15	4.95	0.180	50°	1.44
Sheet Metal Cascade	3.54	11	3.54	0.188	50°	1.47

In the absence of a wing the flat plate compares less favourably with the aerofoil cascade since the interference drag of the flat plate is much reduced. The sheet metal cascades are considerably less effective than the aerofoil cascade but still have some advantage over the flat plate.

Lift increments due to the brakes are plotted in Fig.19a. It will be seen that around $\theta = 50°$ the cascades produce about as much lift as drag, while the flat plate produces maximum lift at about $\theta = 30°$ and zero lift at $\theta = 75°$. This is in good agreement with the results obtained on the 4.5 in. diameter body (Fig.10) the value of X/ℓ for the tests on the 7 in. diameter body being 3.87.

Pitching moment increments are shown in Fig.20. The flat plate gives a maximum trim change at $\theta = 30°$ and zero trim change at $\theta = 73°$. These results are also in good agreement with the measurements made on the 4.5 in. body and given in Fig.14. The cascade brakes give very large trim changes so that it would always be necessary to use them in pairs.

The results of the measurements with a normal hot wire in a plane 15 in. downstream of the brake hinges are shown in Figs.21 and 22. Fig.21 shows that the wake of the cascade brake (at 50°) is split into two regions of low velocity; Fig.22 shows that the longitudinal velocity fluctuations are entirely random. One analysis of the longitudinal velocity fluctuations behind the square flat plate at 70° was made in a position (shown in Fig.22) where the fluctuations are a maximum. The resulting spectrum is shown in Fig.22. This clearly shows the regular shedding of turbulent eddies with associated random low frequency fluctuations larger than those behind the cascade.

The longitudinal fluctuations will not directly affect the aeroplane except via fluctuating forces on the brake itself; the lateral fluctuations have not yet been measured, though work on this is now in hand. On the assumptions that the lateral fluctuations vary directly with the longitudinal fluctuations and that low frequency vibrations are the most important, the cascade brakes look very promising.

If two flat plates, of the same total area, had been used on either side of the body, the spectrum would have been moved to the right by $\log \sqrt{2}$ and the fluctuation maxima would have been beyond the trailing edge of each brake, extending over the width of the brake, in much the same way as for the cascade brakes. At $100f/U_0 = 10$ the relative values of $fF(f)$ would have been 0.002 for the flat plates against 0.0008 for the cascades.

If the fluctuations affect the tailplane, the single flat plate may have an advantage in having its maximum fluctuations below the aircraft and further away from the tail.

5 Discussion

The present results suggest that considerable improvements in low frequency vibration due to flat plate air brakes would result from using the brakes at smaller angles than is usual. A single under fuselage brake has been considered because it interferes least with a tailplane if this is above the fuselage. Such a brake used at small angles suffers from two disadvantages: in order to maintain the same drag a greater area is required, and it is impossible to avoid large trim changes. A possible solution is to use a pair of brakes (on opposite sides of the body, for example) but this will generally bring the wakes of the brakes nearer to the tailplane and increase the blockage effect on trim and elevator hinge moment, and also increase vibration. From stability considerations, tail planes behind swept wings should be low and an obvious solution would be extending the jet pipe and carrying a symmetrical arrangement of brakes behind the tail. When symmetrical arrangements of brakes are considered, cascades offer the advantages of high drag coefficients with relatively small low frequency velocity fluctuations.

6 Conclusions

The nature of the wake behind an isolated square flat plate changes in character between $\theta = 40^\circ$ and 50°. At larger angles there is a regular shedding of turbulent eddies which gives large velocity fluctuations in the wake at a single frequency. Large random low frequency fluctuations are associated with this shedding. At smaller angles there is no regular shedding and the largest random fluctuations occur at relatively high frequency.

Results obtained with a square plate on a body suggest that under these conditions the angle at which the flow changes is greater than that for the isolated plate.

A single brake under a body can give zero trim change only at an angle of about 70°. At angles much different from 70° it is necessary to use a pair of brakes.

A cascade brake has a higher maximum drag coefficient than a flat plate and there is no regular shedding. The lift on a cascade brake produces large changes of trim unless a pair of brakes is used.

<u>List of Symbols</u>

θ	=	Incidence of plate (or brake) relative to free stream or body axis (degrees)
ℓ	=	Length of side of square brake
d	=	Maximum diameter of body
W	=	Width of cascade brake
X	=	Distance of brake hinge plane from end of body or in the case of the body with faired tail, the distance of the brake hinge plane from the datum shown in Fig.7
X_1	=	Distance of C.G. from end of body or, in the case of the body with faired tail, the distance of the C.G. from the datum shown in Fig.7
x	=	Distance from end of body, or, in the case of the body with faired tail, the distance from the datum shown in Fig.7
Z	=	Distance of brake hinge below body axis
S_B	=	Area of plate or brake (see para 4.3) sq.ft
C	=	Cross sectional area of tunnel working section (sq.ft)
A	=	Aspect ratio of plate
U_o	=	Tunnel speed (uncorrected for blockage) ft/sec
U	=	Local mean longitudinal velocity (ft/sec)
u	=	r.m.s. value of longitudinal velocity fluctuation (ft/sec)
ΔL_{100}	=	Lift increment due to plate or brake (lb at 100 ft/sec M.S.)
ΔD_{100}	=	Drag increment due to plate or brake (lb at 100 ft/sec M.S.)
ΔM_{100}	=	Pitching moment increment due to plate or brake (lb ft at 100 ft/sec) M.S.
ΔC_{L_B}	=	Lift increment coefficient $= \dfrac{\Delta L}{qS_B}$
ΔC_{D_B}	=	Drag increment coefficient $= \dfrac{\Delta D}{qS_B}$
ΔC_{M_B}	=	Pitching moment increment coefficient $= \dfrac{\Delta M}{qS_B \ell}$
f	=	Frequency (cycles/sec)

List of Symbols (Contd)

$\frac{100f}{U_o}$ = Frequency corresponding to tunnel speed of 100 ft/sec

$F(f)$ = Spectrum function such that

$$\left(\frac{u}{U_o}\right)^2 = \int_0^\infty F(f)\, df = \int_{-\infty}^\infty fF(f)\, d(\log f)$$

REFERENCES

No.	Author	Title, etc.
1	R.H. James and J.H. Mitchell	Turbulence Measuring Apparatus R.A.E. Tech.Note No. Inst.949 March, 1946
2	H. Schuh and K.G. Winter	R.A.E. 4 ft × 3 ft Experimental Low Turbulence Wind Tunnel Part II Measurements of longitudinal intensity of turbulence R.A.E. Report No. Aero.2285 August, 1948 ARC 11829
3	P.B. Atkins and R.W. Murphy	Low Speed wind tunnel tests on a new type of air brake suitable for Vampire aircraft Aeronautical Research Laboratories, Australia. Aero Note 106 August, 1952
4	Von O. Flachsbart	Messungen an Ebenen und Gewalben Platten Ergenbisse der Aerodynamischen Versuchsanstalt zu Gottingen IV Leiferung 1932 p.96
5	A. Fage and F.C. Johansen	On the flow of air behind an inclined flat plate of infinite span R & M No.1104 February 1927
6	-	Modern Developments in Fluid Dynamics Vol.I para.111
7	E.C. Maskell	Pressure distributions illustrating flow reattachment behind a forward mounted flap C.P. 211 March 1954

TABLE I

Increments of lift, drag and pitching moment

Square plate on 4.50 in. dia. body (Bluff tail) $\frac{\ell}{d} = \frac{2}{3}$, $\frac{Gap}{\ell} = \frac{1}{5}$

X/ℓ	Z/ℓ	θ^o	ΔC_{L_B}	ΔC_{D_B}	ΔC_{M_B}
7.183	0.767	30 50 70 90	0.639 0.370 -0.045 -0.458	0.611 0.864 1.161 1.303	-0.436 0.043 0.970 1.325
4.950	0.767	30 50 70 90	0.584 0.360 -0.037 -0.446	0.610 0.872 1.183 1.342	-0.297 0.073 0.909 1.302
4.167	0.767	90	-0.507	1.353	1.289
3.583	0.767	30 50 50 70 90 110 130	0.558 0.292 0.298 -0.116 -0.509 -0.788 -0.856	0.625 0.895 0.892 1.213 1.338 1.213 0.969	-0.254 0.227 0.277 1.061 1.264 1.080 0.491
3.450	0.767	90	-0.522	1.339	1.311
2.667	0.767	30 50 70 90	0.584 0.224 -0.145 -0.503	0.642 0.931 1.187 1.308	-0.207 0.389 1.057 1.149
2.083	0.767	30 50 70 90	0.510 0.233 -0.017 -0.368	0.679 0.953 1.207 1.294	-0.164 0.444 0.903 1.008
1.500	0.767	30 50 70 90 90	0.542 0.467 0.271 -0.128 -0.120	0.697 0.979 1.300 1.359 1.355	-0.107 0.326 0.590 0.691 0.716
0.910	0.767	30 50 70 90	0.829 0.962 0.804 0.346	0.818 1.327 1.613 1.573	0.251 0.651 0.902 0.793
0.323	0.767	30 50 70 90	0.960 1.187 1.062 0.750	0.800 1.401 1.714 1.798	0.545 0.734 0.965 1.165

TABLE II

Increments of lift, drag and pitching moment

Square plate on 4.50 in. dia. body (Boat tail) $\frac{\ell}{d} = \frac{2}{3}$, $\frac{Gap}{\ell} = \frac{1}{5}$ and $\frac{2}{5}$

X/ℓ	Z/ℓ	θ^o	$Gap/\ell = 1/5$			$Gap/\ell = 2/5$		
			ΔC_{L_B}	ΔC_{D_B}	ΔC_{M_B}	ΔC_{L_B}	ΔC_{D_B}	ΔC_{M_B}
8.707	0.767	30	0.689	0.611	-0.757	0.872	0.673	-1.231
		50	0.455	0.844	-0.317	0.519	0.868	-0.664
		50	0.447	0.851	-0.299			
		70	-0.016	1.141	0.870	0.074	1.105	0.258
		90	-0.445	1.285	1.391	-0.373	1.242	0.930
8.123	0.767	90	-0.441	1.274	1.286	-	-	-
		110	-0.674	1.153	1.000	-	-	-
		130	-0.859	0.929	0.615	-	-	-
6.363	0.767	30	0.667	0.624	-0.470	0.894	0.683	-1.008
		50	0.433	0.878	0.030	0.500	0.872	-0.405
		70	-0.010	1.165	0.985	0.046	1.113	0.546
		90	-0.425	1.298	1.373	-0.381	1.256	0.959
4.040	0.733	30	-	-	-	0.895	0.722	-0.793
		30	0.633	0.632	-0.278	0.892	0.720	-0.771
		50	0.416	0.919	0.440	0.467	0.891	-0.062
		70	-	-	-	0.066	1.166	0.868
		70	0.031	1.236	1.109	0.064	1.165	0.857
		90	-0.370	1.356	1.432	-0.316	1.306	1.009
		90	-0.364	1.350	1.383	-	-	-
		110	-0.657	1.196	1.128	-	-	-
		130	-0.848	0.982	0.565	-	-	-
2.357	0.663	30	0.716	0.667	-0.198	0.917	0.764	-0.634
		50	-	-	-	0.491	0.916	0.037
		50	0.451	0.954	0.410	0.486	0.923	0.013
		70	-	-	-	0.272	1.201	0.451
		70	0.226	1.231	0.793	0.266	1.208	0.442
		90	-0.138	1.328	0.884	-0.098	1.320	0.694
		90	-0.121	1.333	0.906	-	-	-
		110	-0.519	1.175	0.809	-	-	-
		130	-0.761	0.929	0.206	-	-	-
1.007	0.567	90	0.371	1.510	0.309	-	-	-
		90	0.387	1.510	0.289			
		110	-0.040	1.290	0.382	-	-	-
		110	-0.033	1.290	0.359			
		130	-0.490	0.820	0.173	-	-	-
		130	-0.487	0.834	0.217			
0.867	0.547	30	0.873	0.753	-0.010	1.056	0.824	-0.451
		50	1.018	1.257	0.008	1.001	1.220	-0.420
		70	0.812	1.492	0.132	0.807	1.536	-0.245
		90	0.449	1.526	0.167	0.432	1.597	-0.133

TABLE III

Increments of lift, drag, and pitching moment.

Square plate on 4.50 in. dia. body (Faired tail) $\frac{\ell}{d} = \frac{2}{3}$, $\frac{Gap}{\ell} = \frac{1}{5}$

X/ℓ	Z/ℓ	θ°	ΔC_{L_B}	ΔC_{D_B}	ΔC_{M_B}
8.707	0.767	30 50 70 90	0.661 0.419 -0.045 -0.426	0.618 0.860 1.131 1.263	-0.706 -0.154 1.032 1.342
6.363	0.767	30 50 70 90	0.652 0.409 -0.036 -0.425	0.600 0.869 1.149 1.267	-0.530 0.061 1.059 1.334
4.040	0.733	30 50 70 90	0.676 0.437 0.039 -0.350	0.622 0.891 1.200 1.328	-0.367 0.224 1.113 1.419
2.357	0.663	30 50 70 70 90	0.720 0.488 0.182 0.168 -0.223	0.630 0.931 1.205 1.210 1.333	-0.345 0.246 0.788 0.802 1.009
0.867	0.547	30 50 70 90	0.748 0.611 0.322 -0.031	0.630 0.925 1.189 1.274	-0.237 0.275 0.405 0.582

TABLE IV

Increments of lift, drag and pitching moment

Square plate on 4.50 in. dia. body (Boat tail) $\frac{\ell}{d} = \frac{1}{2}$, $\frac{Gap}{\ell} = \frac{1}{5}$

X/ℓ	Z/ℓ	θ^o	ΔC_{L_B}	ΔC_{D_B}	ΔC_{M_B}
11.609	1.022	30	0.528	0.577	-0.757
		50	0.382	0.866	-0.165
		70	-0.087	1.183	1.565
		70	-0.079	1.169	1.516
		90	-0.436	1.295	1.976
8.484	1.022	30	0.497	0.565	-0.348
		50	0.370	0.882	0.103
		70	-0.043	1.196	1.479
		70	-0.044	1.195	1.426
		90	-0.424	1.301	2.057
5.387	0.978	30	0.462	0.563	0.083
		50	0.326	0.925	0.747
		70	-0.008	1.267	1.766
		90	-0.407	1.372	2.120
3.142	0.884	30	0.531	0.602	0.161
		50	0.370	0.946	0.839
		50	0.365	0.958	0.841
		70	0.099	1.271	1.486
		90	-0.282	1.361	1.724
1.155	0.729	30	0.850	0.766	0.289
		50	1.036	1.338	0.605
		70	0.872	1.608	0.767
		90	0.500	1.612	0.927

TABLE V

Increments of lift, drag and pitching moment.
Cascade brakes on 7 in. dia. body

θ^o	ΔL_{100}	ΔD_{100}	ΔM_{100}
5 in. Square Plate			
16.7	1.17	0.48	-2.35
24.4	1.72	1.00	-3.07
29.7	1.84	1.35	-3.40
33.7	1.60	1.44	-3.07
36.7	1.40	1.42	-2.59
41.7	1.33	1.54	-2.34
51.7	0.97	1.90	-1.79
71.7	0.17	2.43	-0.09
91.7	-0.58	2.64	1.19
109.7	-1.04	2.38	1.84
Sheet Metal Cascade (W = 5.75")			
30.3	2.20	3.66	-3.77
40.3	3.59	4.46	-6.19
45.3	4.04	4.54	-6.82
50.3	4.22	4.69	-7.42
60.3	4.14	4.32	-7.39
70.3	3.50	3.96	-6.50
90.3	2.39	3.66	-4.97

θ^o	ΔL_{100}	ΔD_{100}	ΔM_{100}
Aerofoil Cascade (W = 5.75")			
30.3	2.01	4.43	-3.58
40.3	2.86	5.38	-6.43
45.3	4.91	5.86	-9.02
50.3	5.95	6.35	-10.61
60.3	6.42	6.04	-11.43
70.3	6.62	5.24	-11.89
90.3	4.07	2.68	-7.53
Sheet Metal Cascade (W = 5.00")			
40.3	2.29	2.79	-3.88
50.3	2.81	3.08	-4.89
60.3	2.56	2.86	-4.97
2 Sheet Metal Cascades (W = 3.54")			
40	0.06	3.07	0.03
50	0.02	3.26	0.04
60	0.06	3.08	0.03

Wt.2078.CP251.K3 - Printed in Great Britain

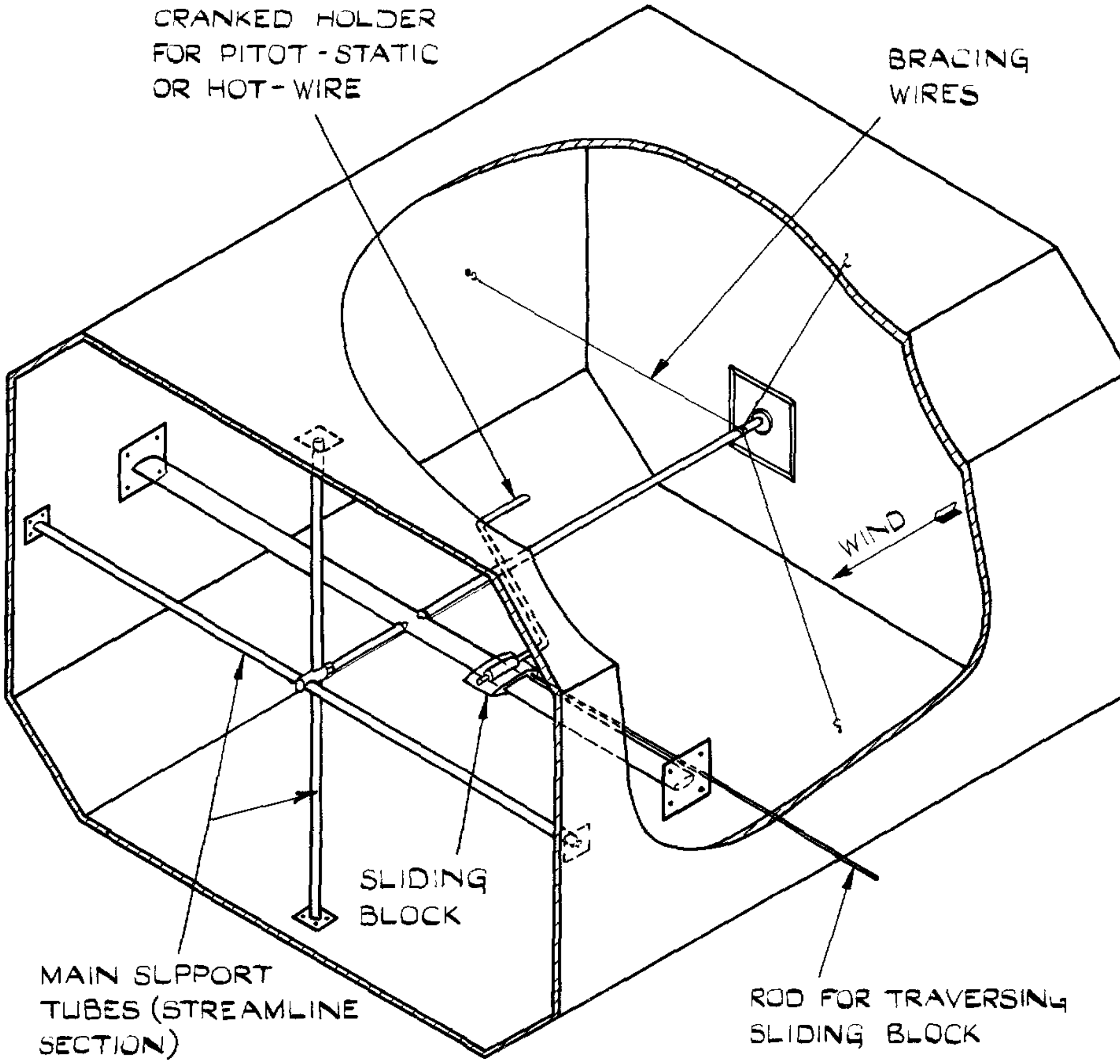

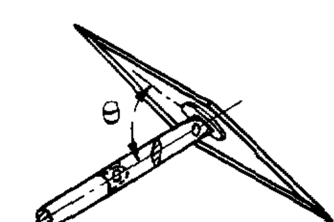

PLATE AT $\theta = 40^\circ$ MOUNTED
ON STREAMLINE STRUT.

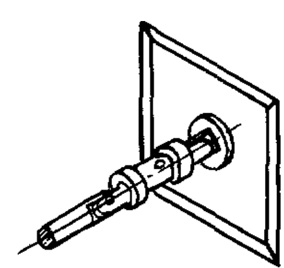

PLATE MOUNTED
ON DRAG BALANCE

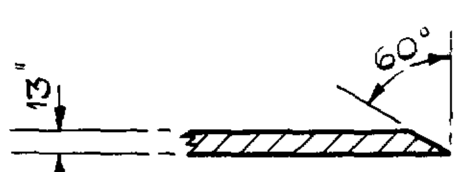

SCRAP SECTION THROUGH
PLATE

FIG.1 ARRANGEMENT OF APPARATUS. TESTS
ON FLAT PLATES IN 4FT. X 3 FT. WIND TUNNEL.

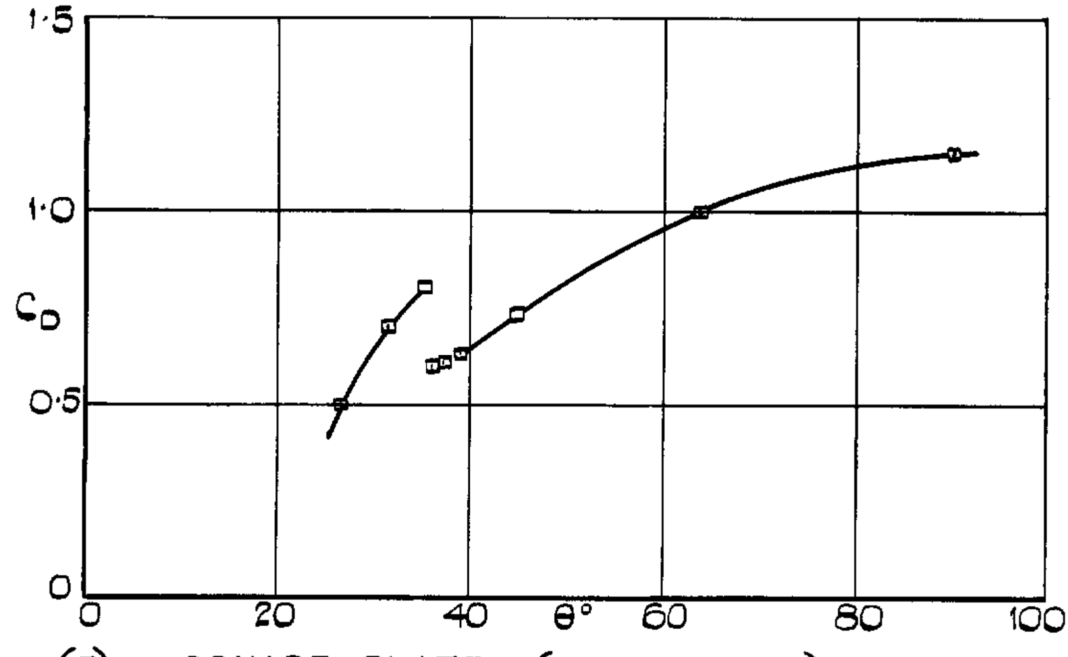

(a) SQUARE PLATE (S_B = 25 SQ IN.)

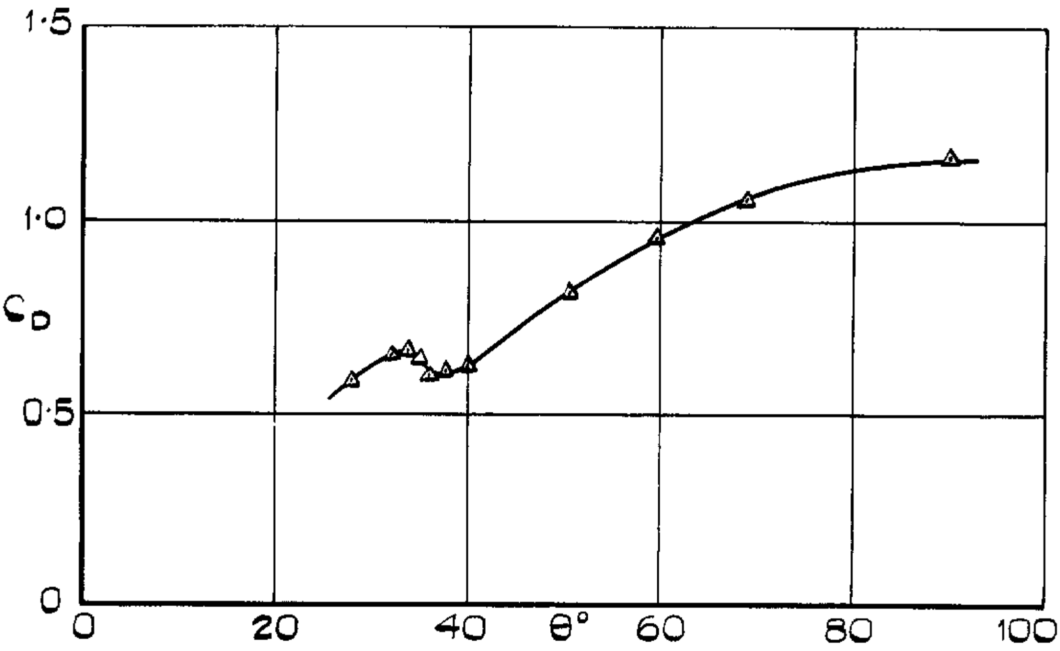

(b) DELTA PLATE (S_B = 25 SQ.IN.)

FIG. 2. (a & b) FLAT PLATES - VARIATION OF DRAG WITH INCIDENCE.

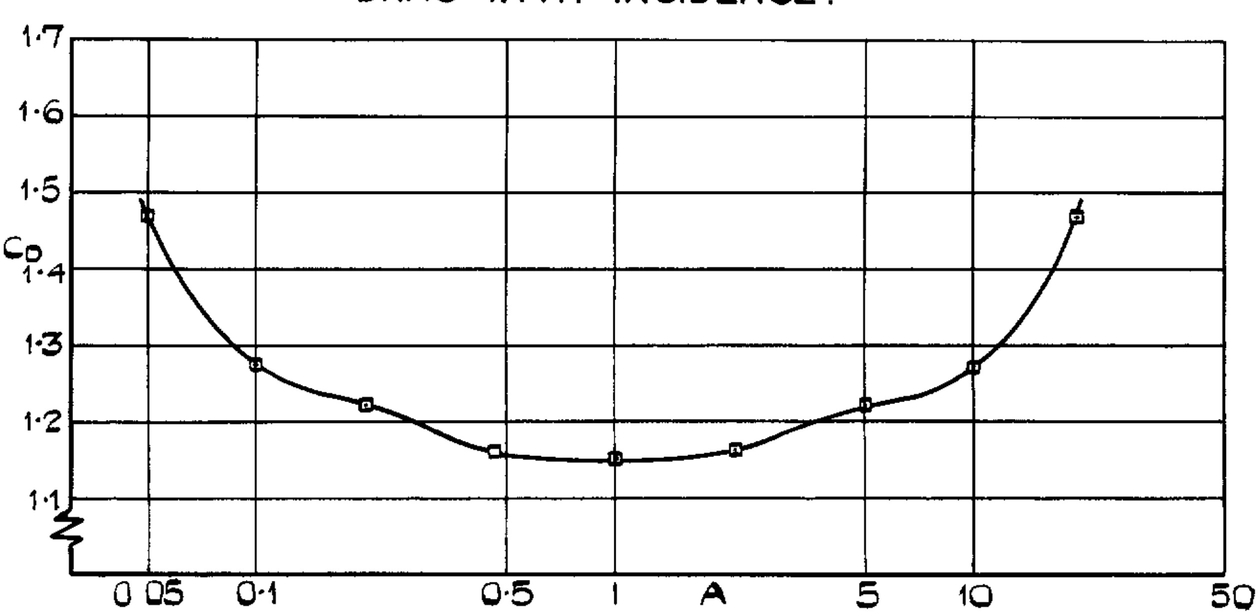

FIG. 3. RECTANGULAR FLAT PLATES (θ = 90°) VARIATION OF DRAG WITH ASPECT RATIO.

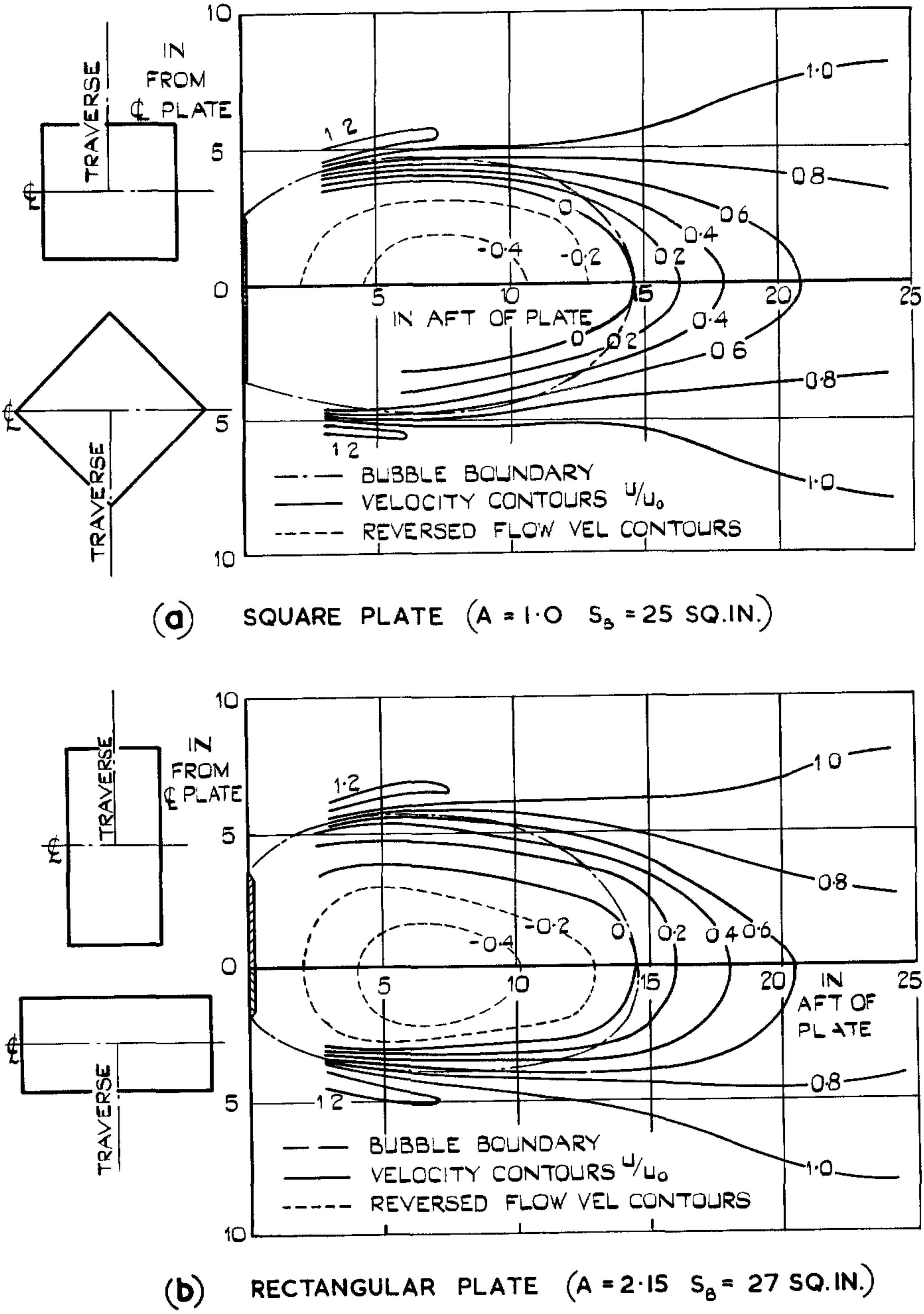

FIG. 4 (a&b) FLOW BEHIND FLAT PLATES
(Θ = 90°)

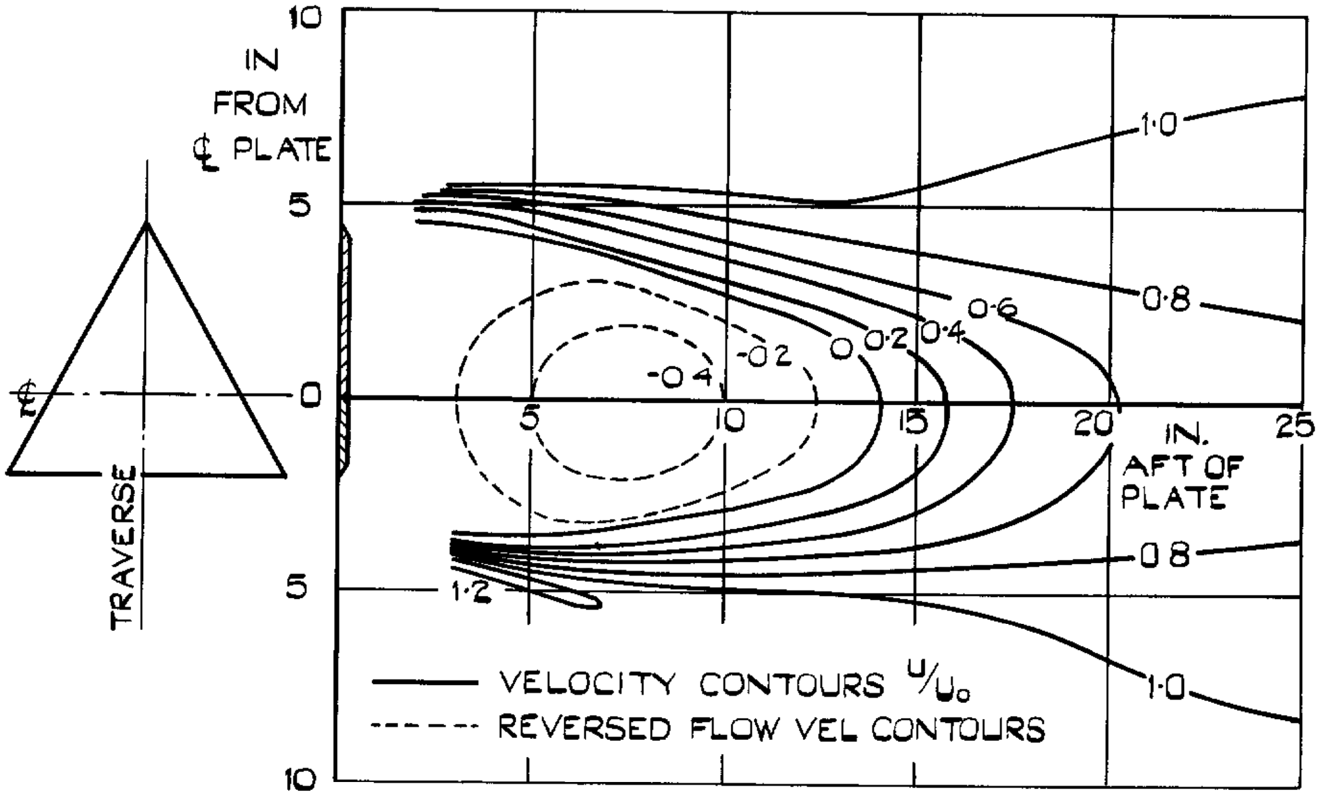

(c) 60° DELTA PLATE (S_B = 25 SQ. IN.)

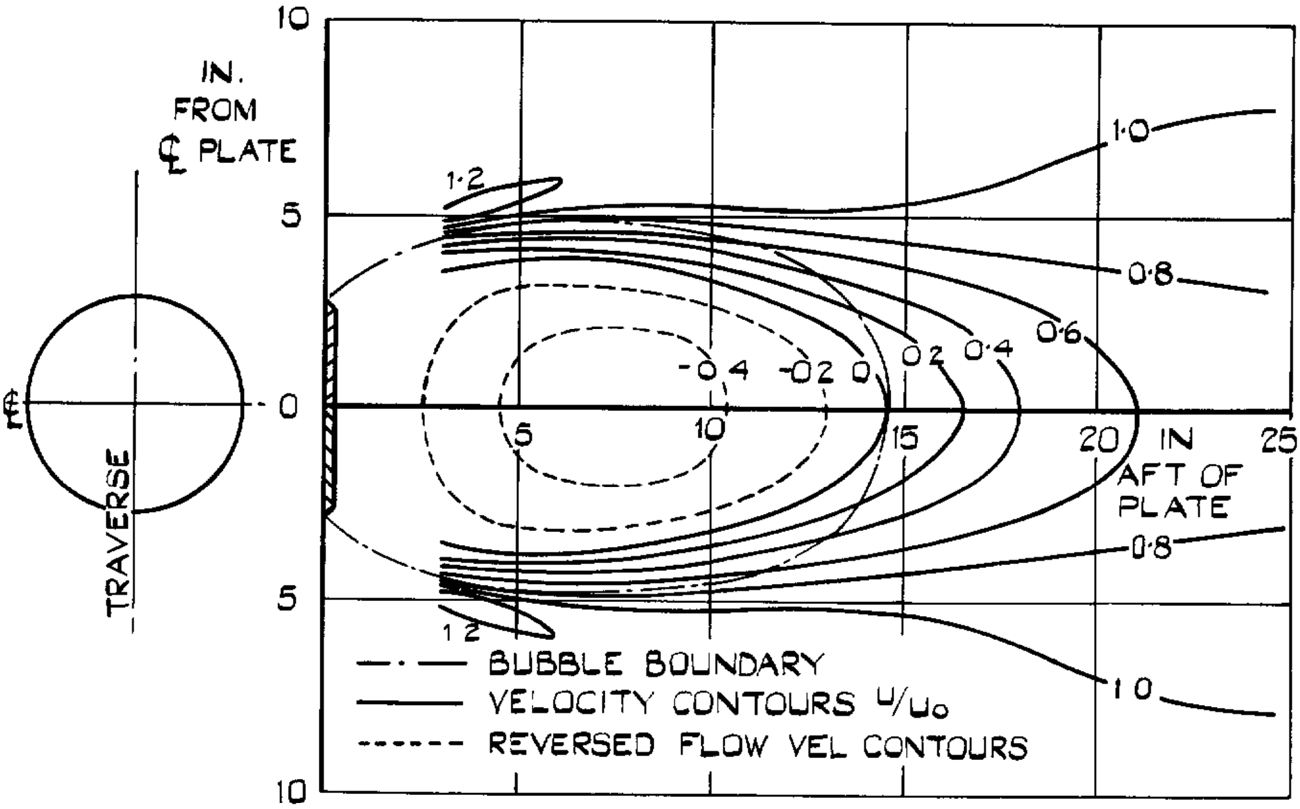

(d) CIRCULAR PLATE (S_B = 25 I SQ. IN.)

FIG. 4.(c&d) FLOW BEHIND FLAT PLATES
(θ = 90°)

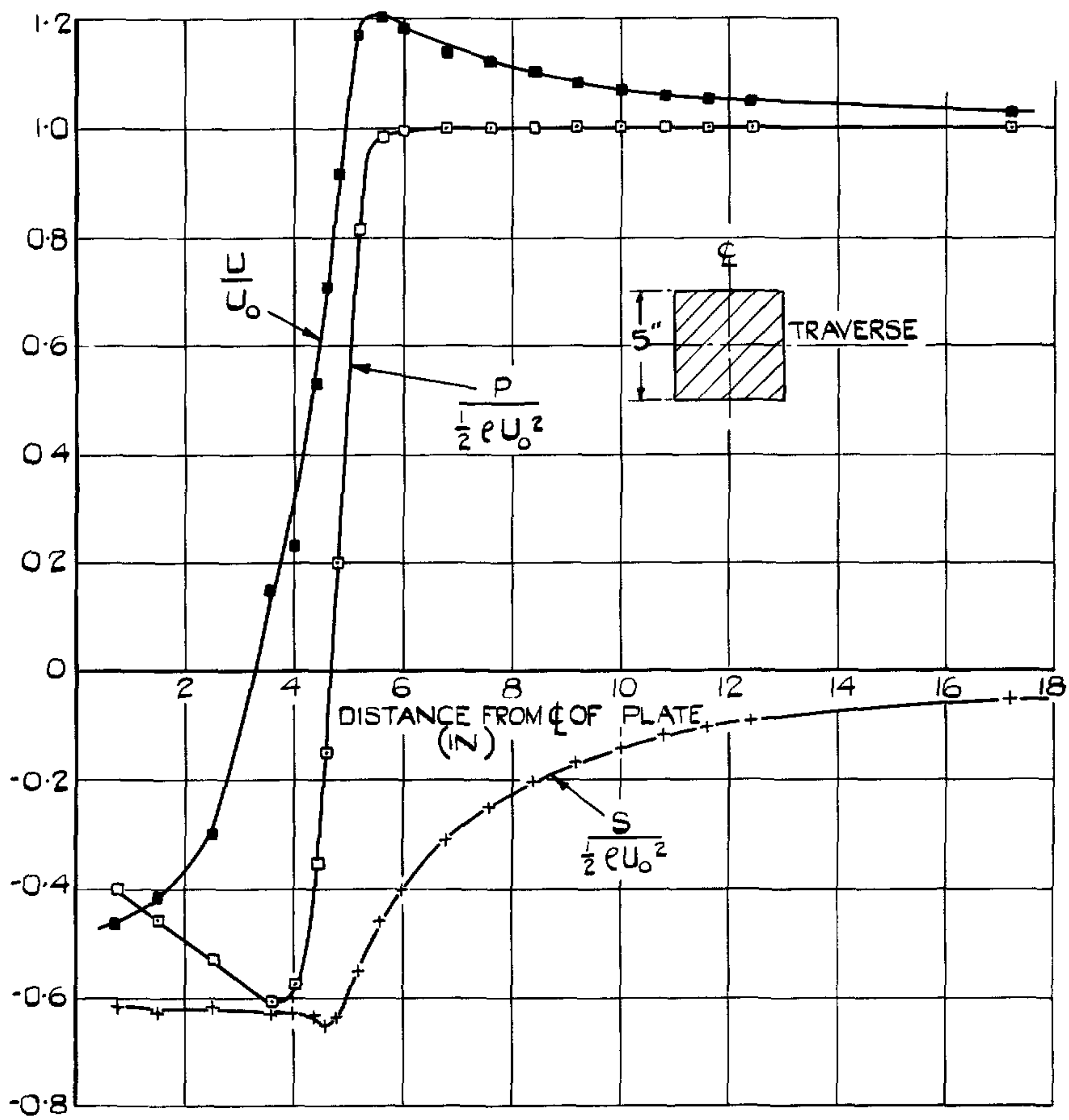

(e) TOTAL HEAD, STATIC PRESSURE AND VELOCITY DISTRIBUTION 6 IN. BEHIND SQUARE PLATE. ($S_B = 25$ SQ. IN.)

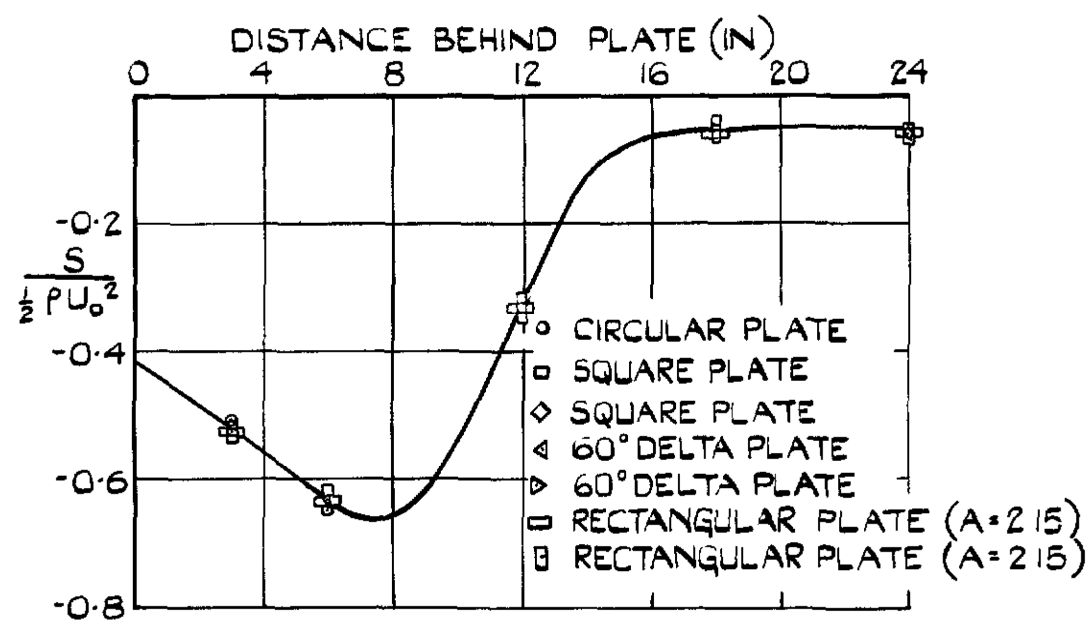

(f) STATIC PRESSURE BEHIND PLATES NEAR PLATE AXIS.

FIG. 4 (e & f) FLOW BEHIND FLAT PLATES ($\theta = 90°$)

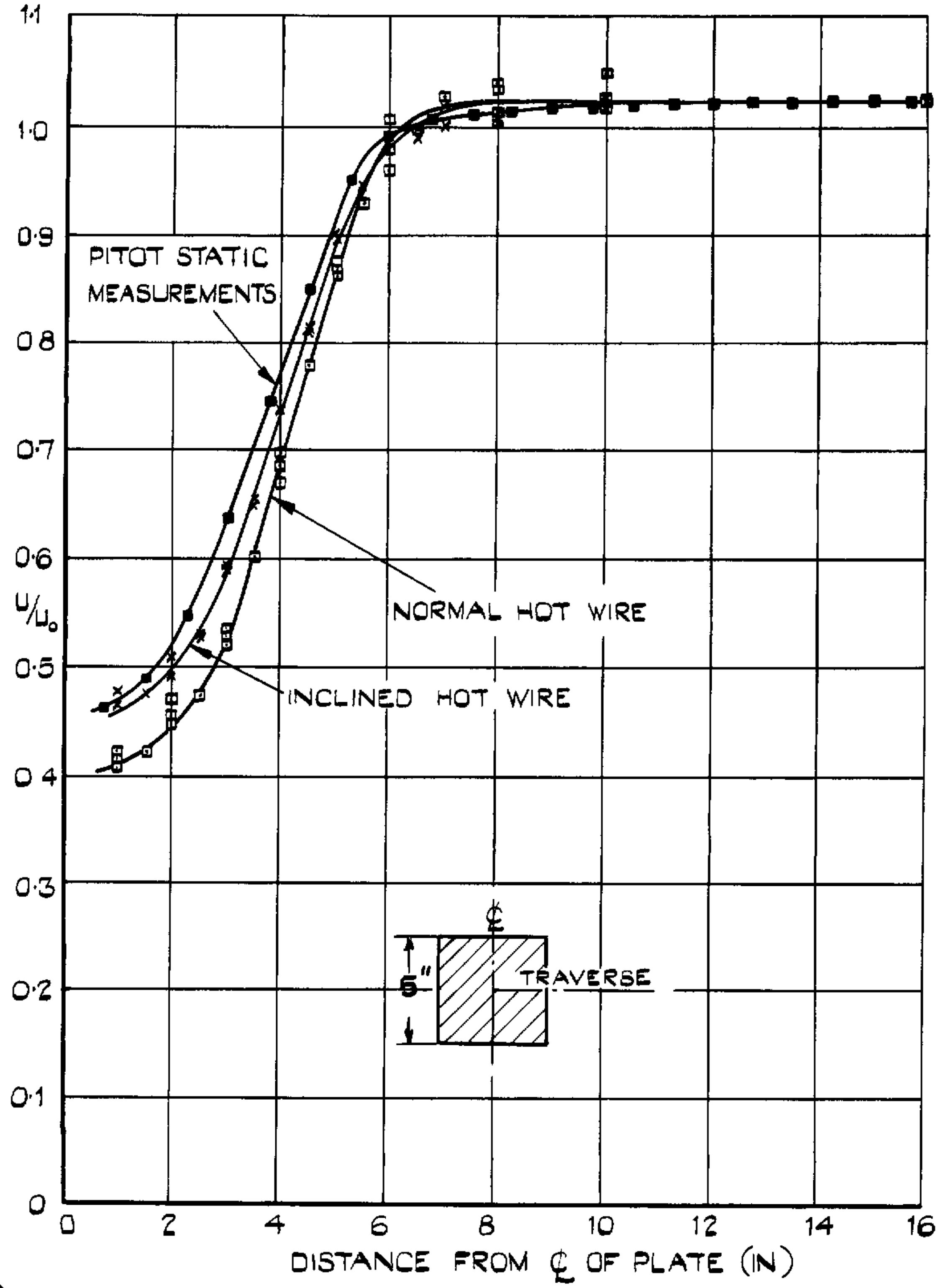

(g) VELOCITY DISTRIBUTION 18·0 IN. BEHIND SQUARE PLATE.

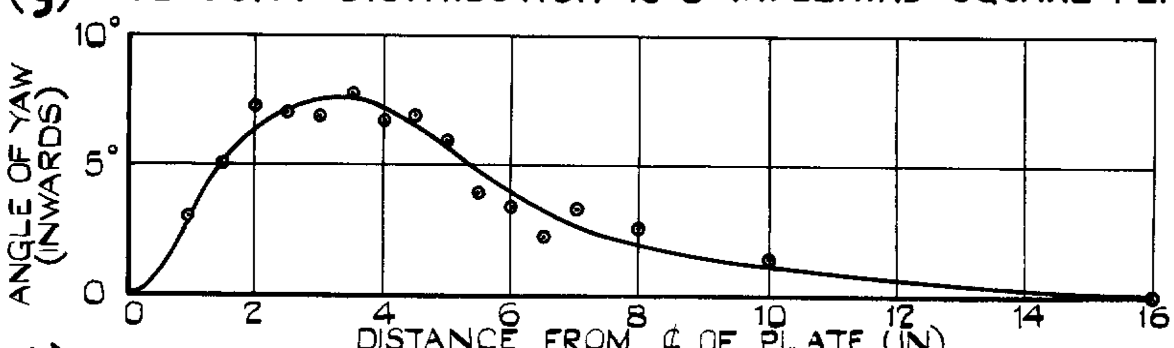

(h) ANGLE OF YAW 18·0 IN. BEHIND SQUARE PLATE (25 SQ.IN.)

FIG. 4.(g&h) FLOW BEHIND FLAT PLATES
(θ = 90°)

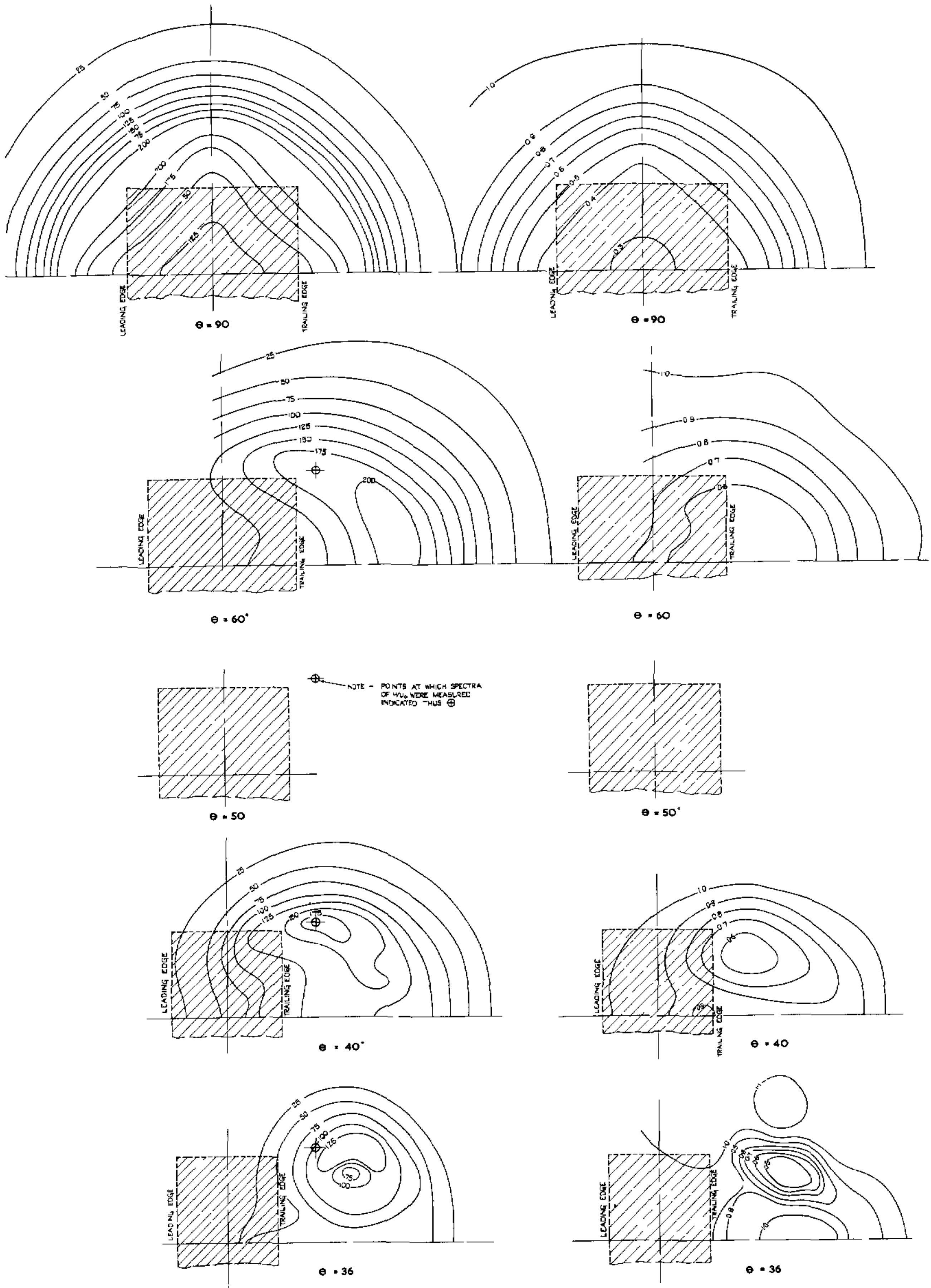

(a) CONTOURS OF $10^3 \frac{u}{U_0}$ (b) CONTOURS OF $\frac{U}{U_0}$

FIG 5 (a & b) FLOW BEHIND SQUARE PLATE 15·3 INCHES DOWNSTREAM

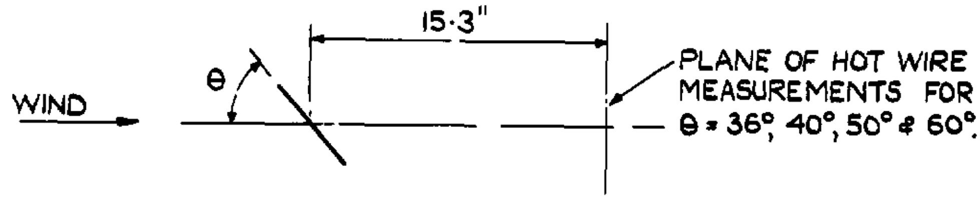

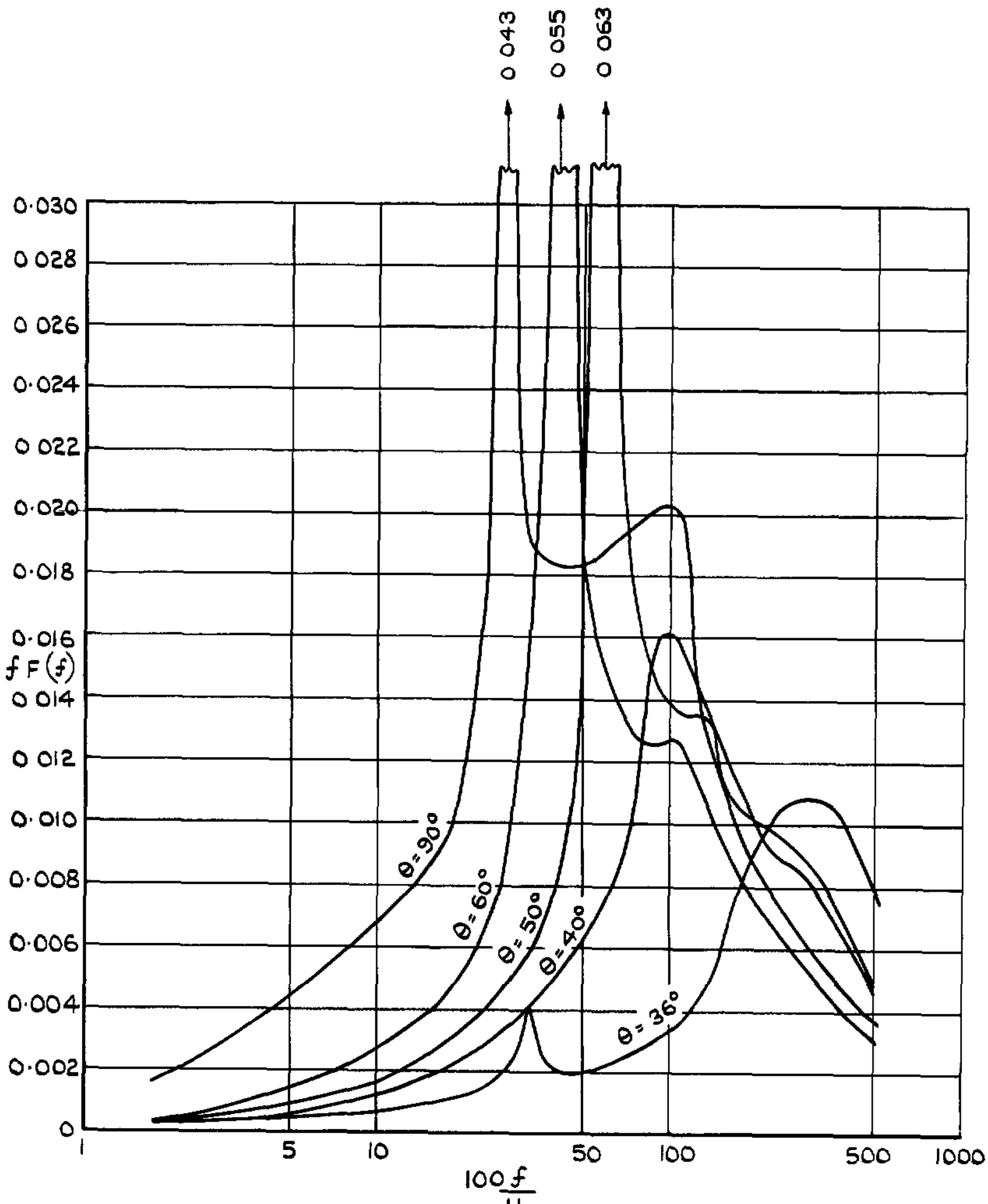

FIG 6. FLOW BEHIND SQUARE PLATE.

SPECTRA OF u/U_0 MEASURED IN PLANE 15·3 IN DOWNSTREAM OF PLATE AT POINTS INDICATED ON FIG 5.
(SPECTRUM FOR θ = 90° MEASURED 11 8 IN DOWNSTREAM AT POINT 5 IN FROM ℄)

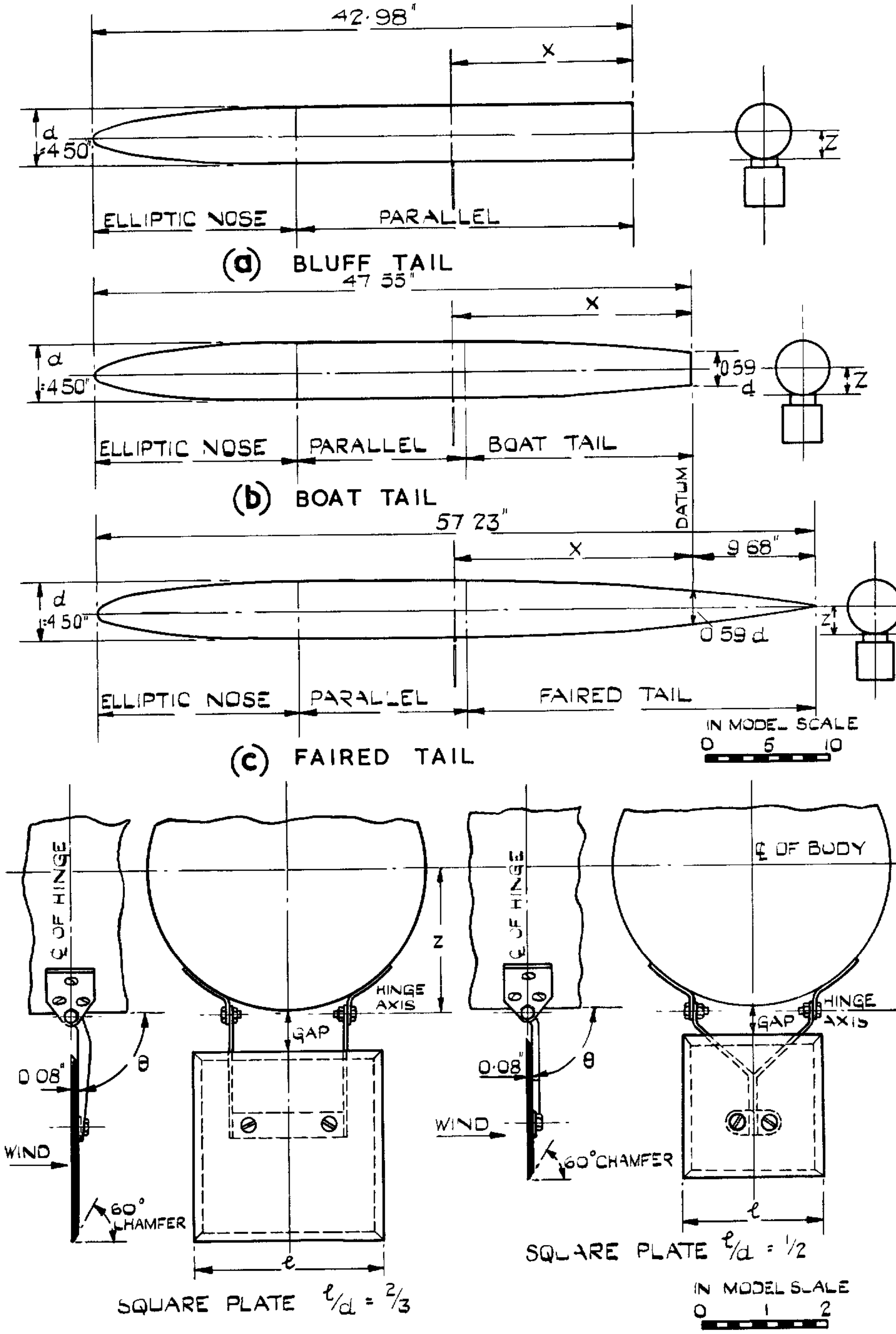

FIG. 7. (a-c). ARRANGEMENT OF SQUARE PLATES ON 4·50 IN. DIA. BODY.

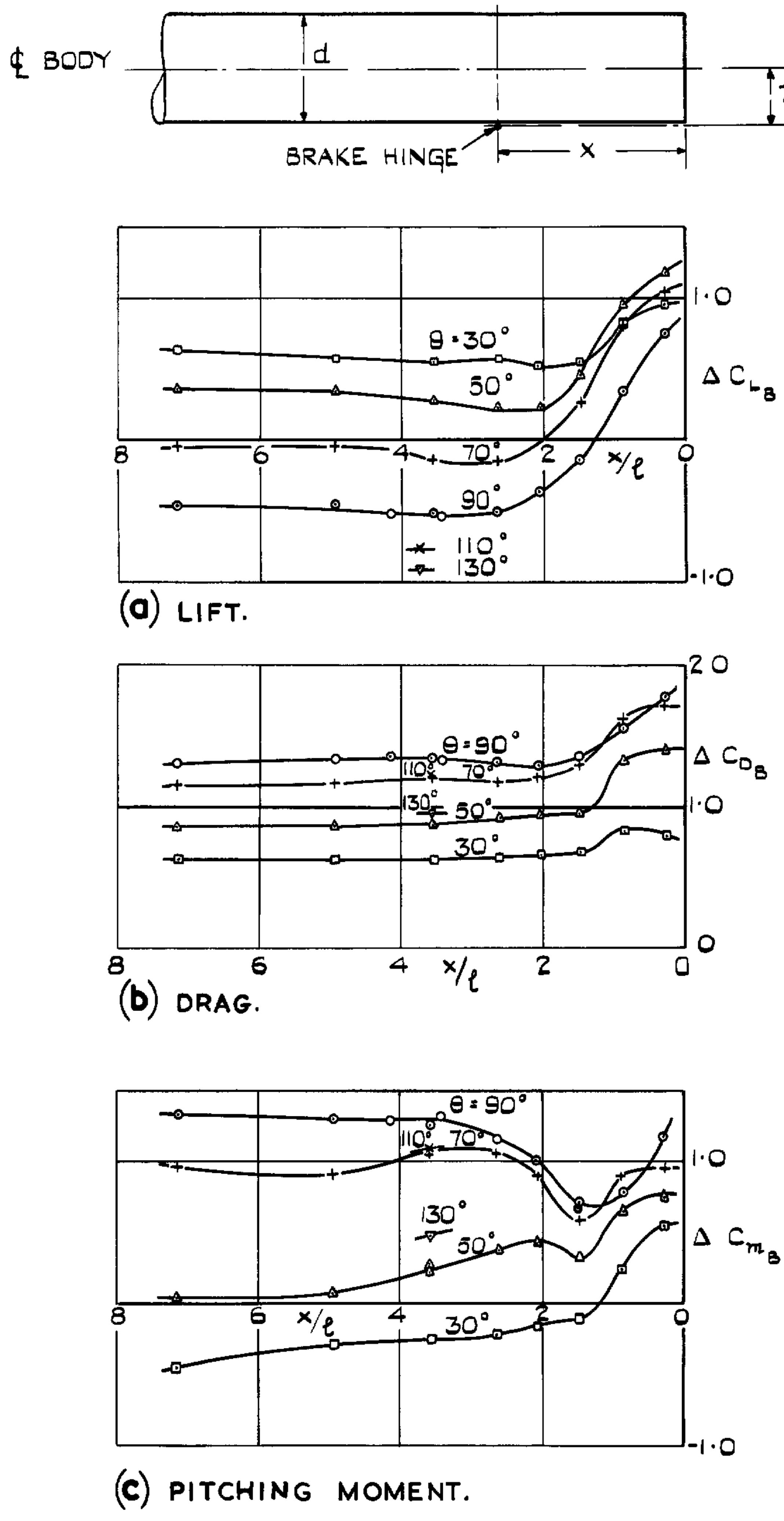

FIG.8 (a – c) LIFT, DRAG AND PITCHING MOMENT SQUARE PLATE ON 4·50 IN. DIA BODY (BLUFF TAIL) $\ell/d = 2/3$, $\frac{GAP}{\ell} = 1/5$.

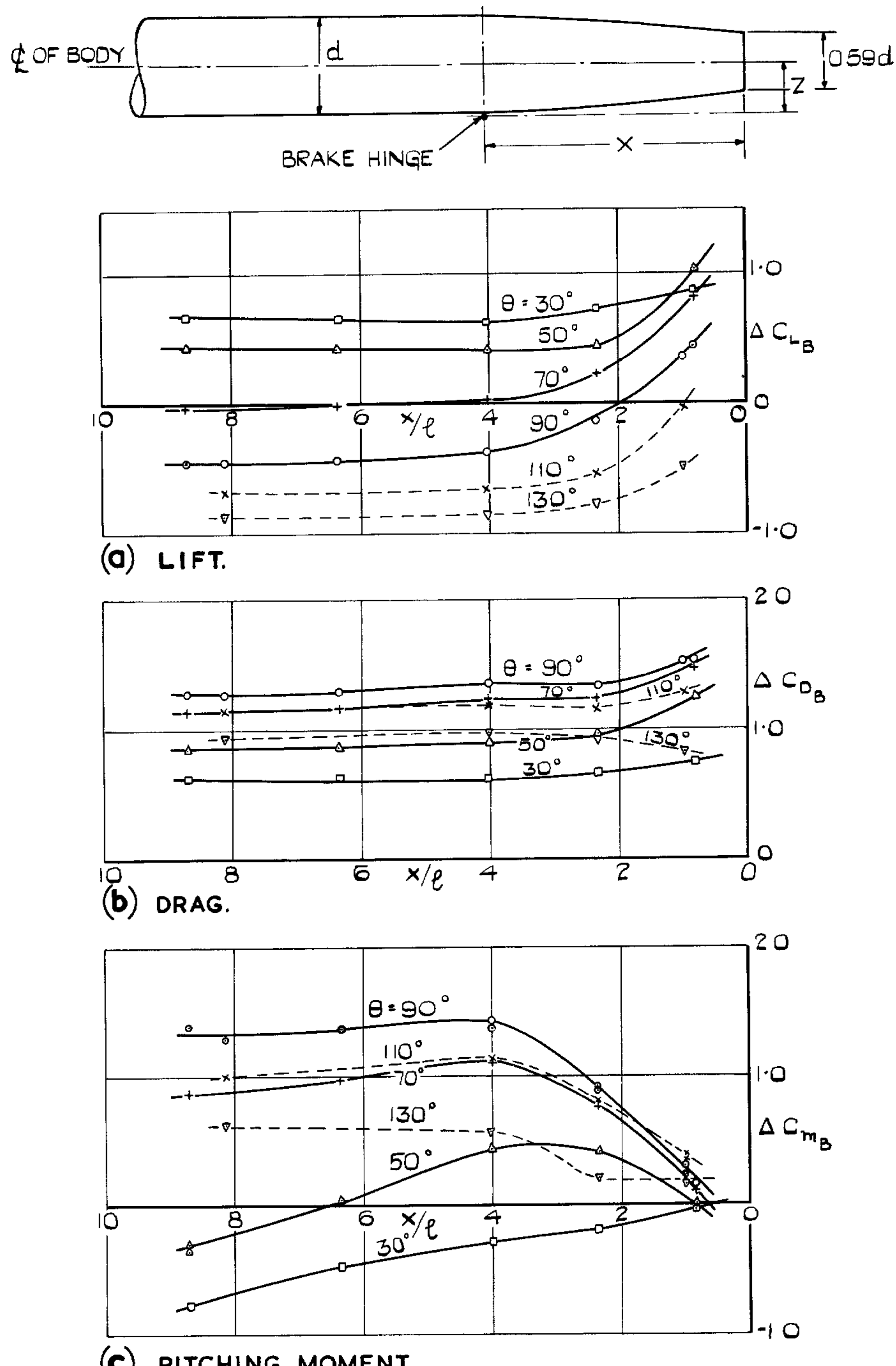

FIG.9 (a–c) LIFT, DRAG AND PITCHING MOMENT SQUARE PLATE ON 4·50IN DIA BODY (BOAT TAIL) $\ell/d = 2/3$, $\frac{GAP}{\ell} = 1/5$

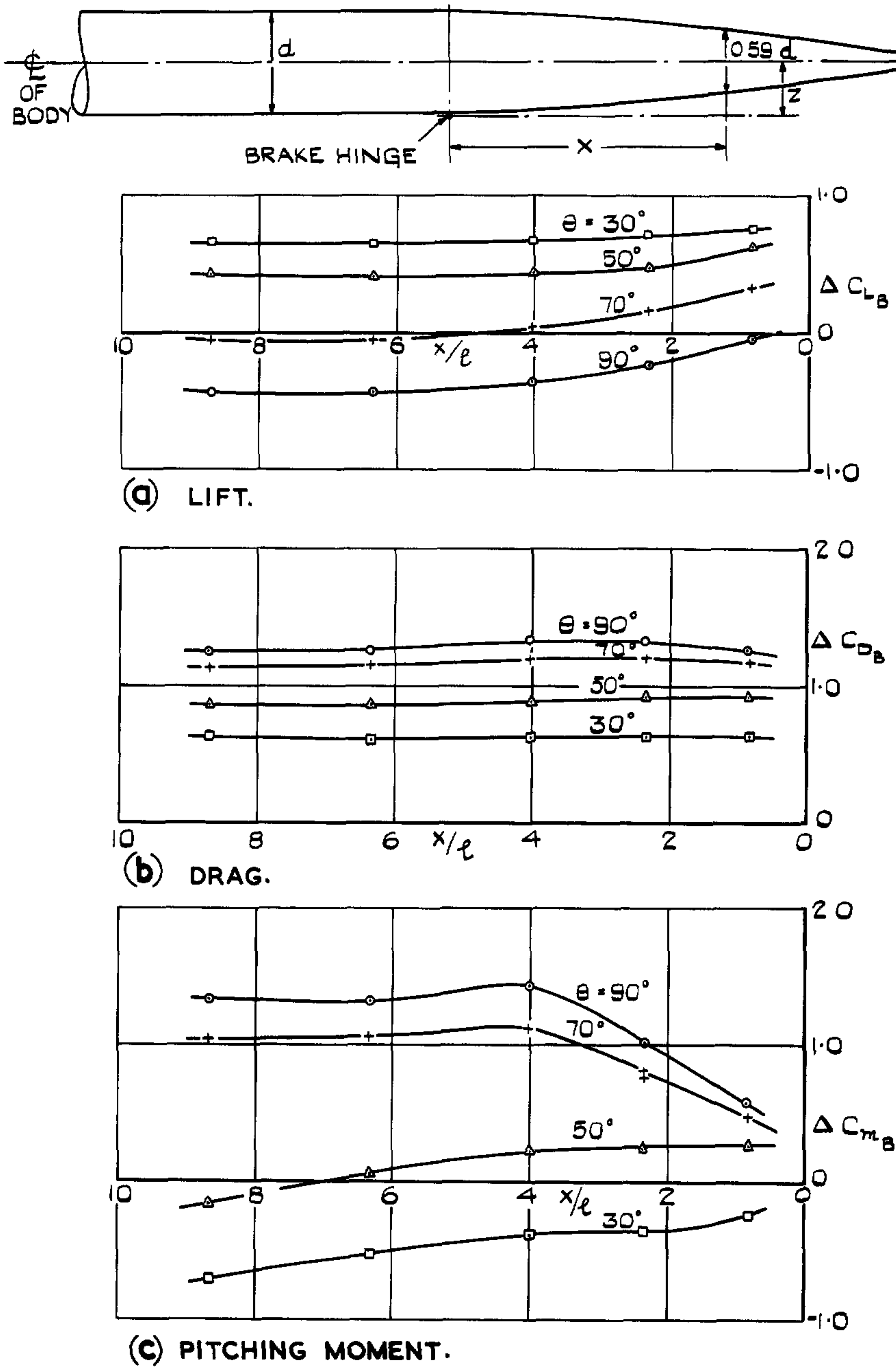

FIG. 10 (a–c) LIFT, DRAG AND PITCHING MOMENT SQUARE PLATE ON 4·50 IN DIA. BODY (FAIRED TAIL) $\ell/d = 2/3$, $\frac{GAP}{\ell} = 1/5$

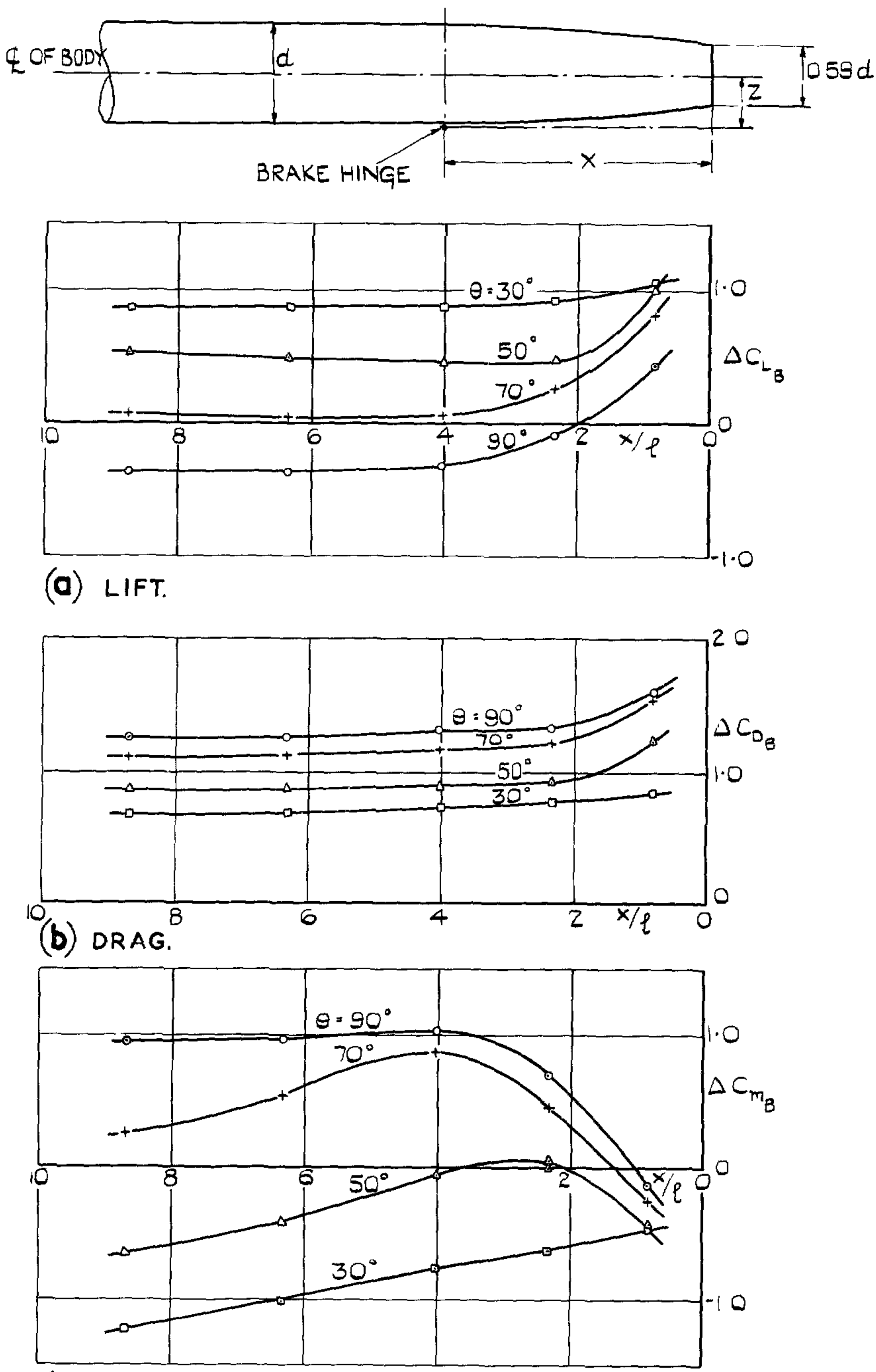

FIG 11 (a-c) LIFT, DRAG AND PITCHING MOMENT
SQUARE PLATE ON 4·50 IN BODY (BOAT TAIL)
$\ell/d = 2/3, \quad \frac{GAP}{\ell} = 2/5$

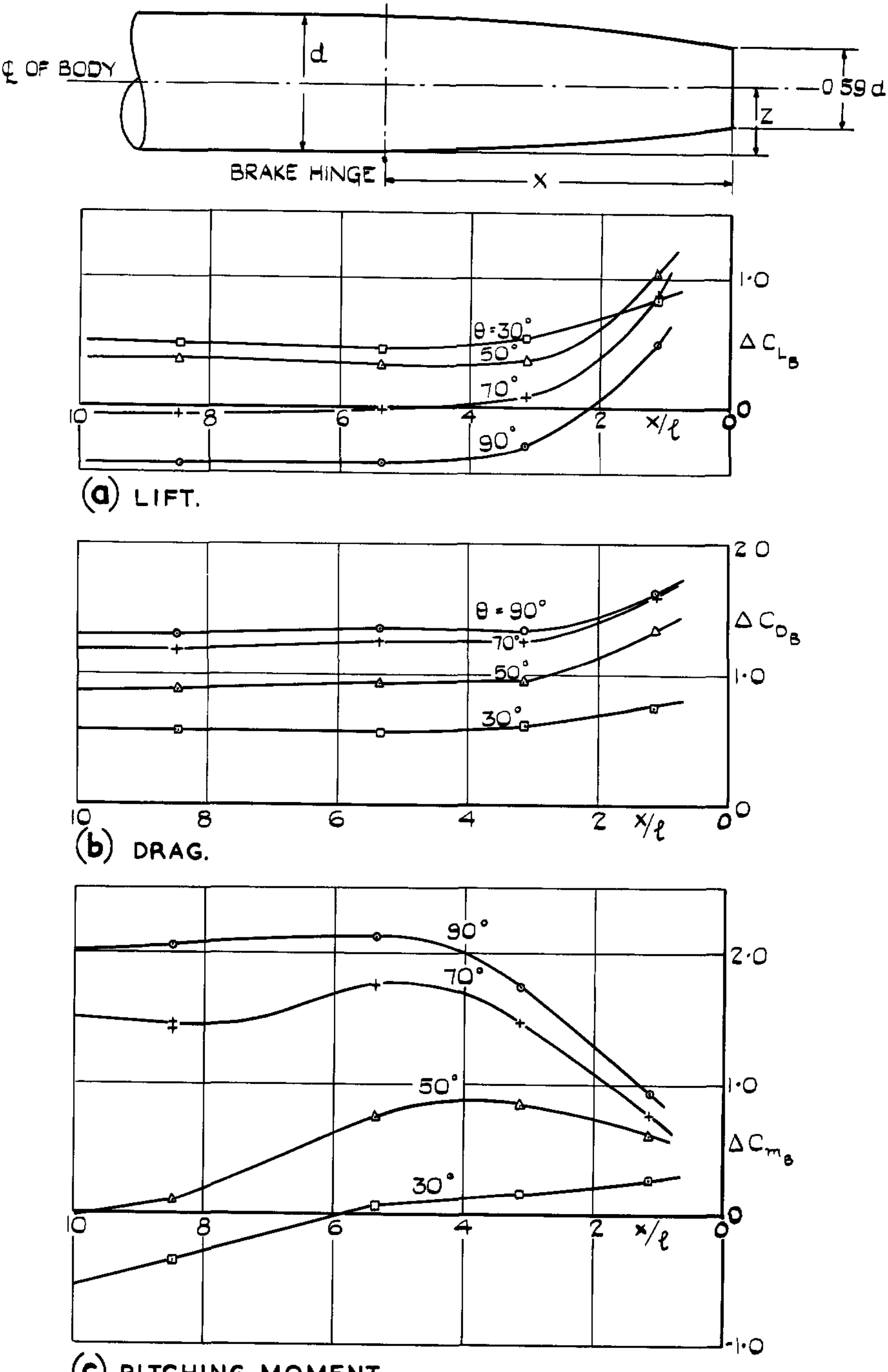

FIG. 12. (a–c) LIFT, DRAG AND PITCHING MOMENT SQUARE PLATE ON 4·50 IN. DIA. BODY (BOAT TAIL) $\ell/d = \frac{1}{2}$ GAP = 1/5.

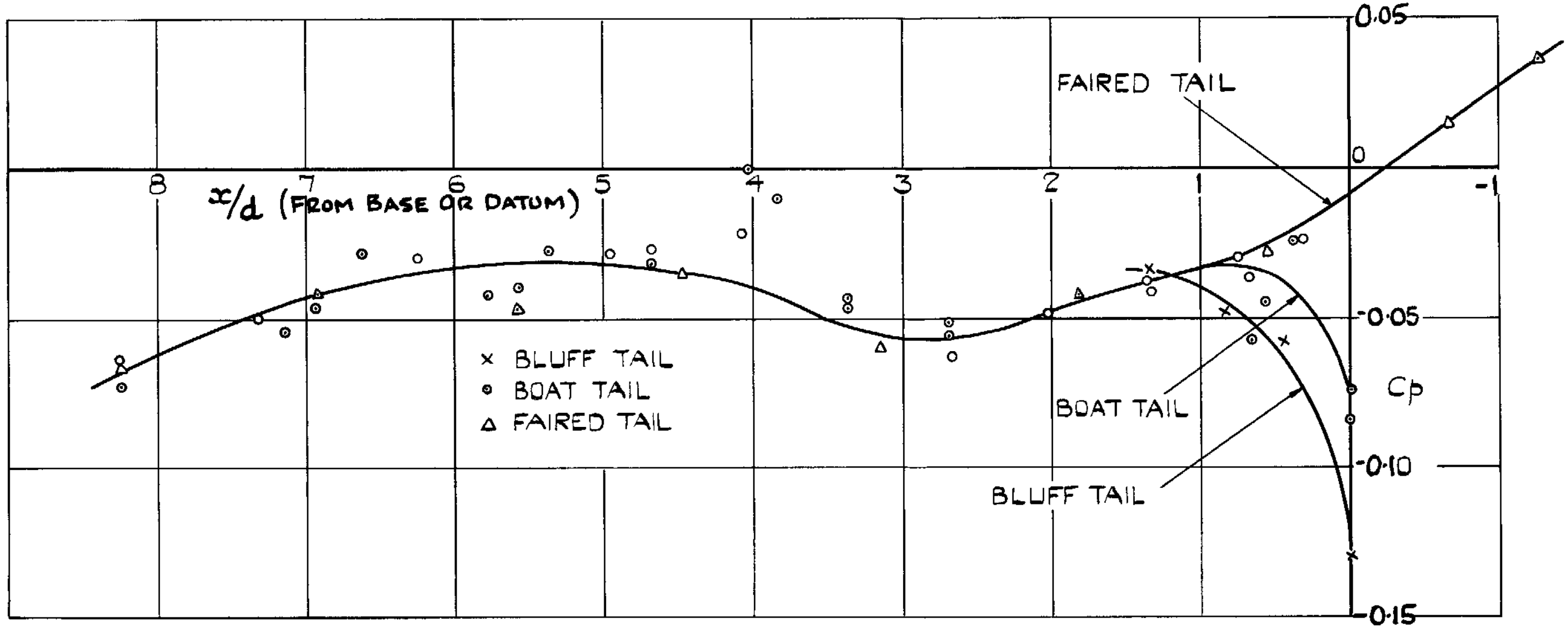

FIG.13. STATIC PRESSURE DISTRUBUTIONS ON 4·5IN. DIA BODY.

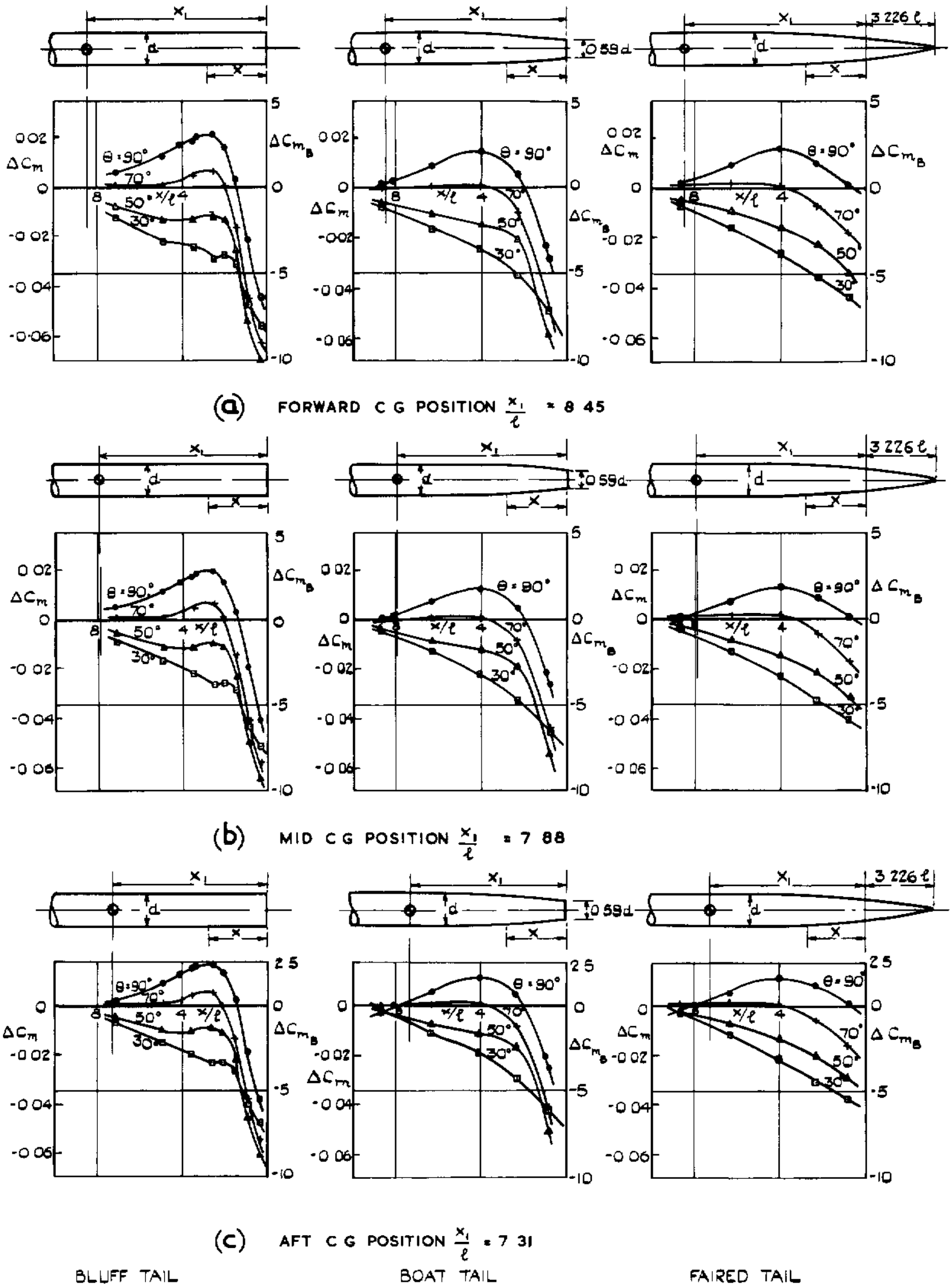

ΔC_m BASED ON HUNTER WING AREA (346 SQ FT) AND MEAN CHORD (10 33 FT) ASSUMING MODEL TO BE $\frac{1}{11\ 66}$ SCALE

d = MAXIMUM BODY DIAMETER
ℓ = LENGTH OF PLATE SIDE

FIG. 14. (a - c). PITCHING MOMENT ABOUT A RANGE OF ASSUMED C.G. POSITION.
SQUARE PLATE ON 4·50 IN. DIA BODY. $\ell/d = 2/3$, $GAP/\ell = 1/5$.

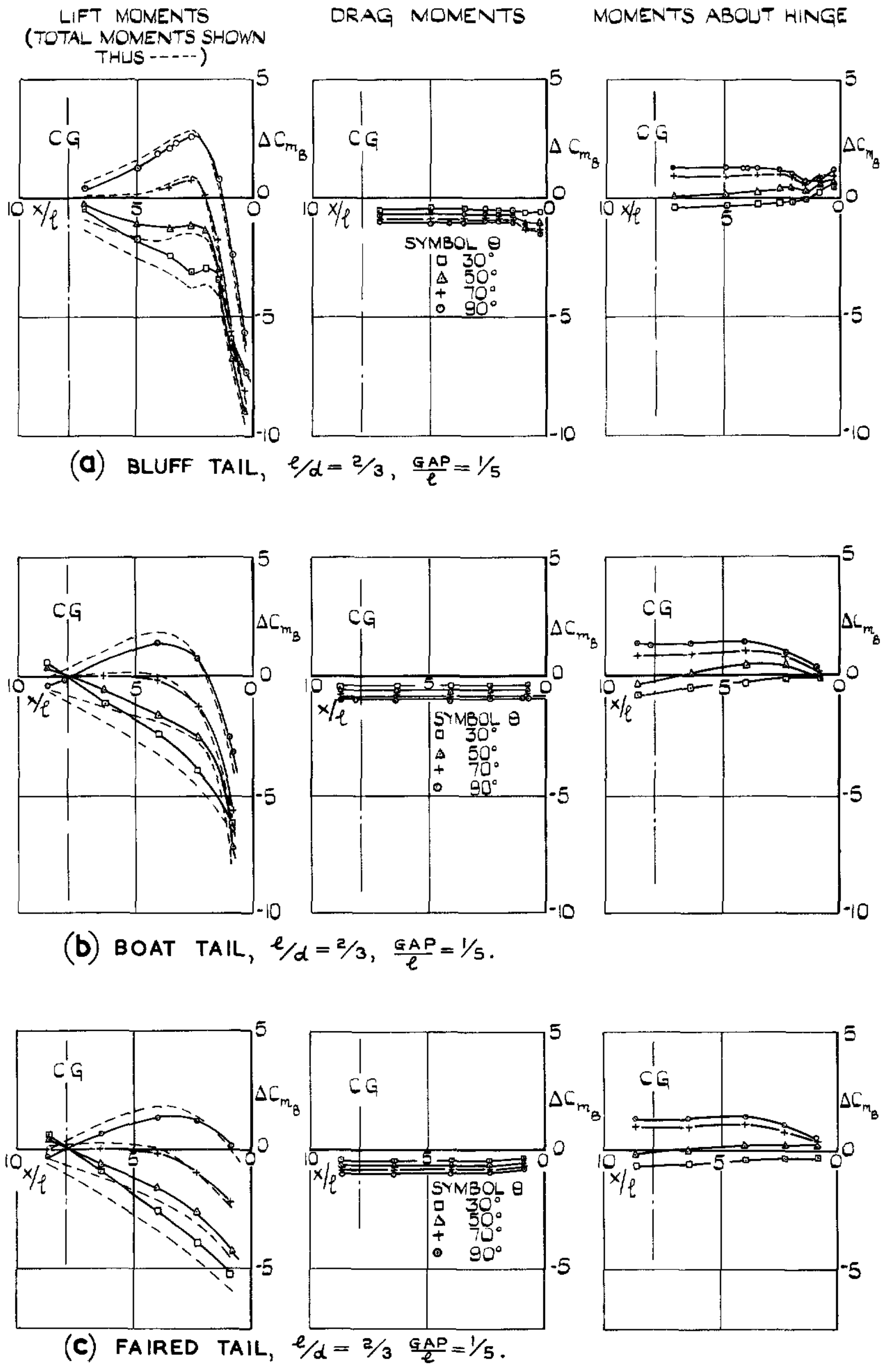

FIG 15 (a-c) ANALYSIS OF PITCHING MOMENT ABOUT MID C G POSITION OF SQUARE PLATE ON 4·50 IN DIA BODY (SEE FIG 14)

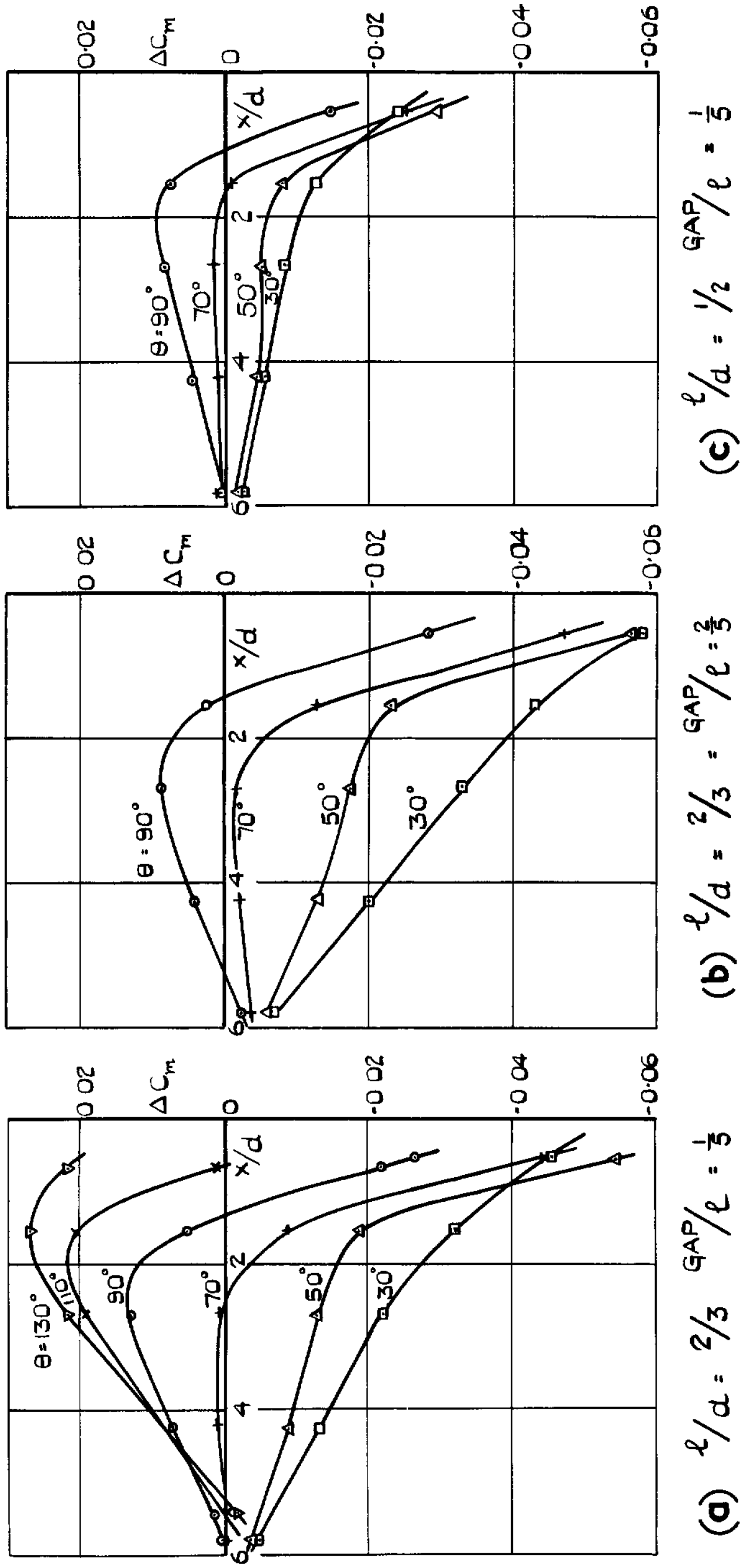

FIG. 16 (a-c) PITCHING MOMENT ABOUT MID C.G. POSITION (FIG. 14.) EFFECT OF GAP AND PLATE SIZE. SQUARE PLATE ON 4·5 INS. DIA. BODY WITH BOAT TAIL.

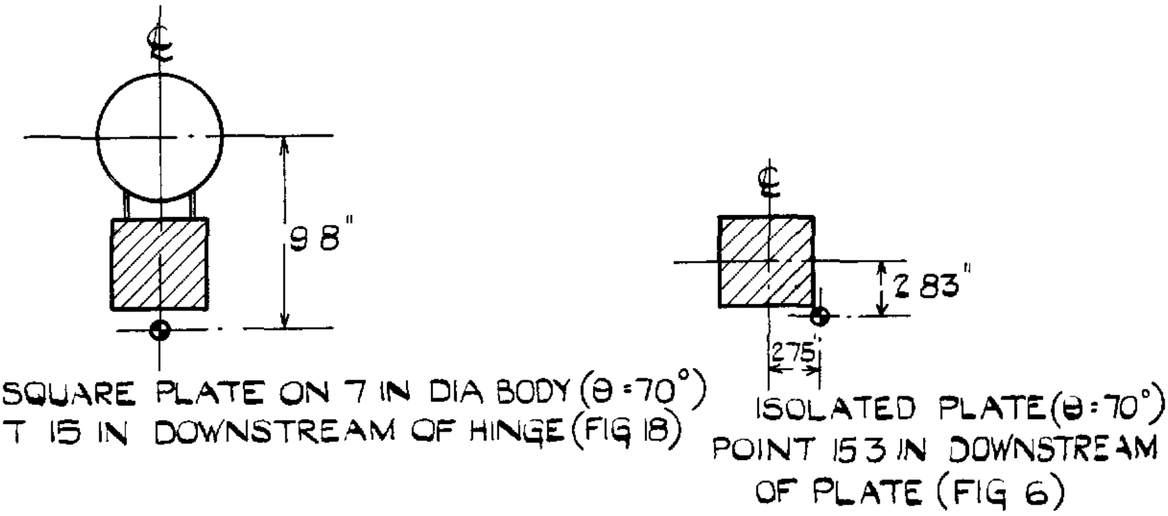

SKETCHES SHOWING POINTS AT WHICH SPECTRA WERE MEASURED OR INTERPOLATED

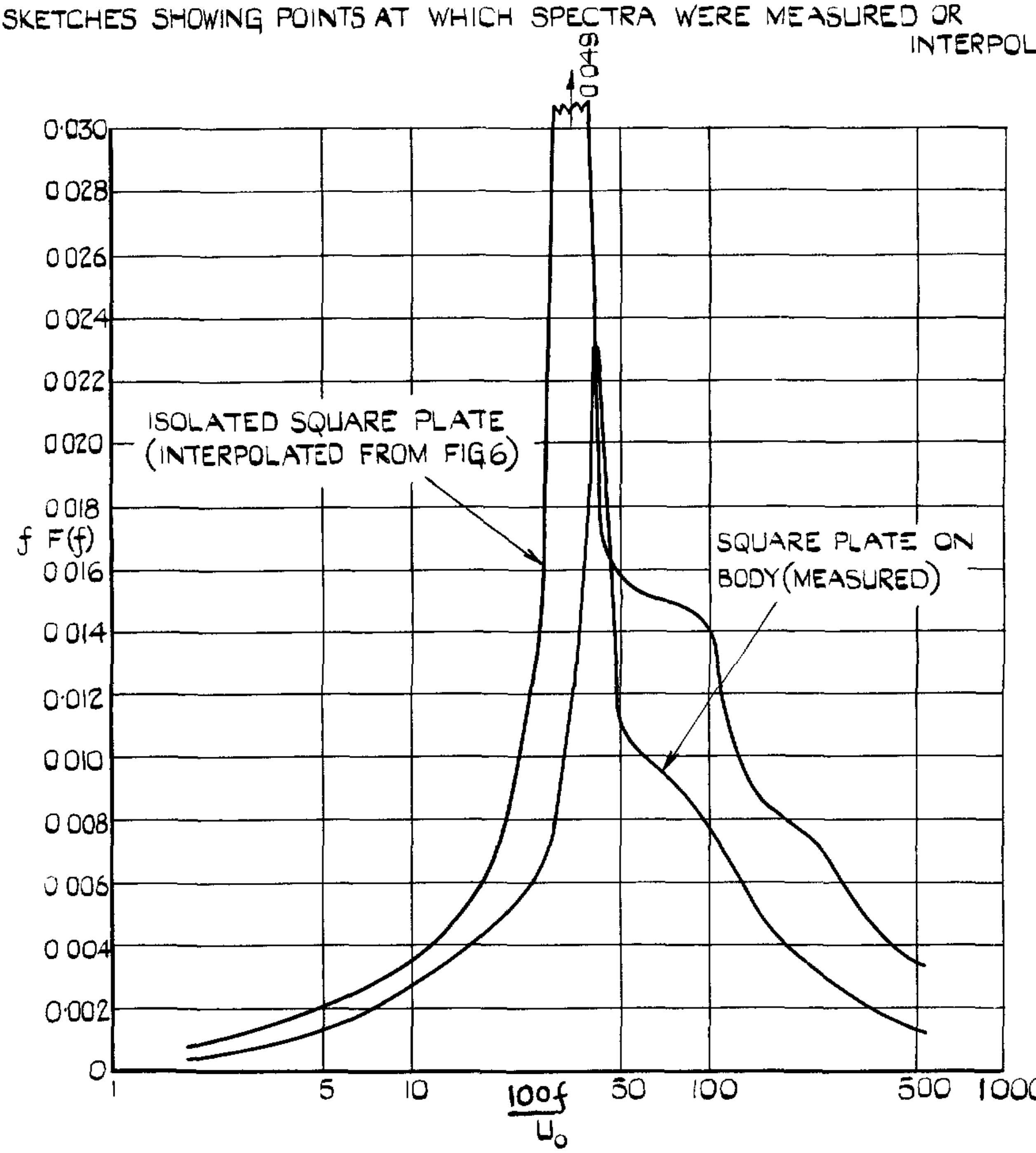

FIG. 17. FLOW BEHIND SQUARE PLATE ($\theta = 70°$) COMPARISON OF SPECTRA OF u/U_0 FOR PLATE ON 7 IN. DIA. BODY & ISOLATED PLATE

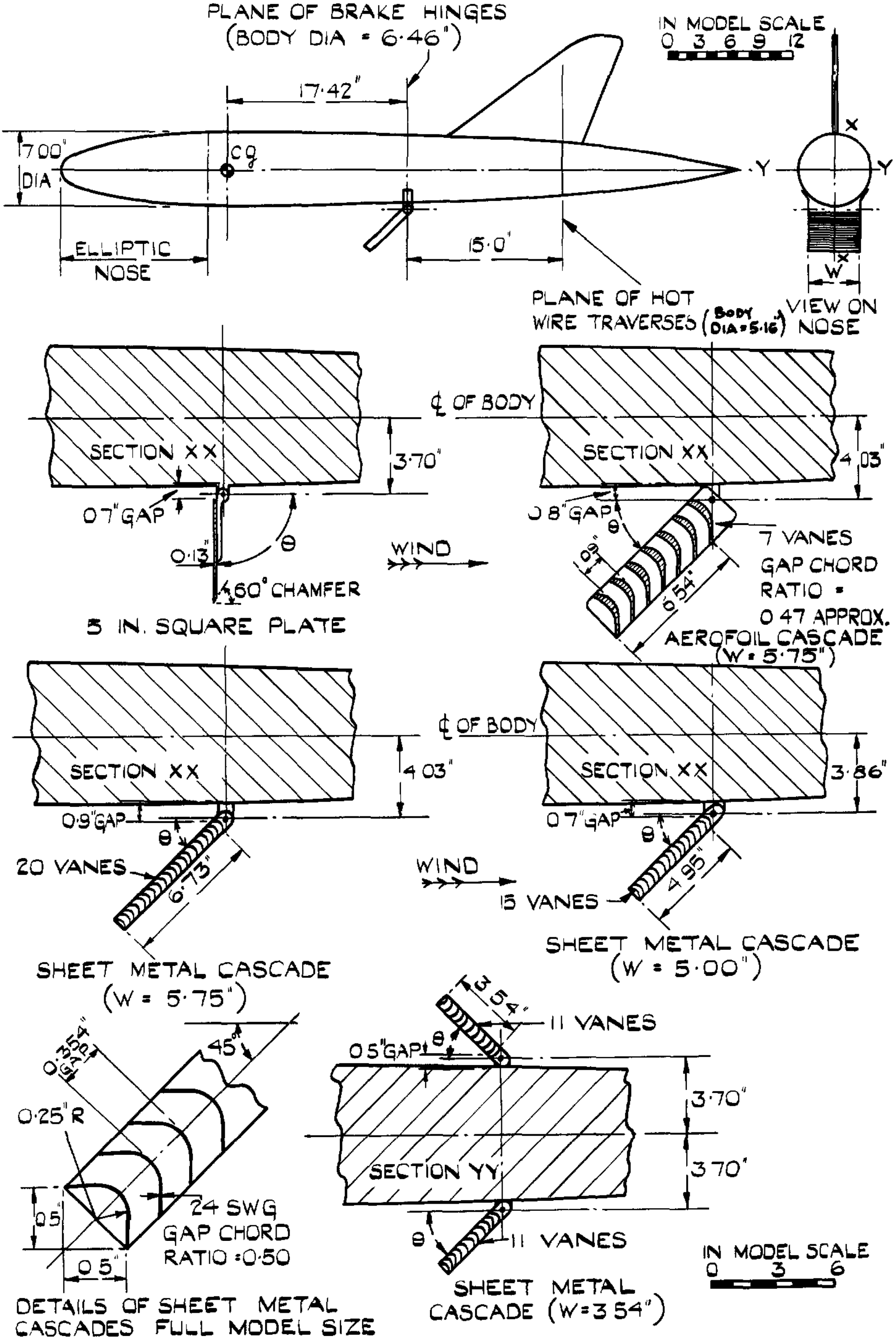

FIG. 18. ARRANGEMENT OF BRAKES ON 7 IN. DIA. BODY.
(CASCADE BRAKES SHOWN AT θ = 45°)

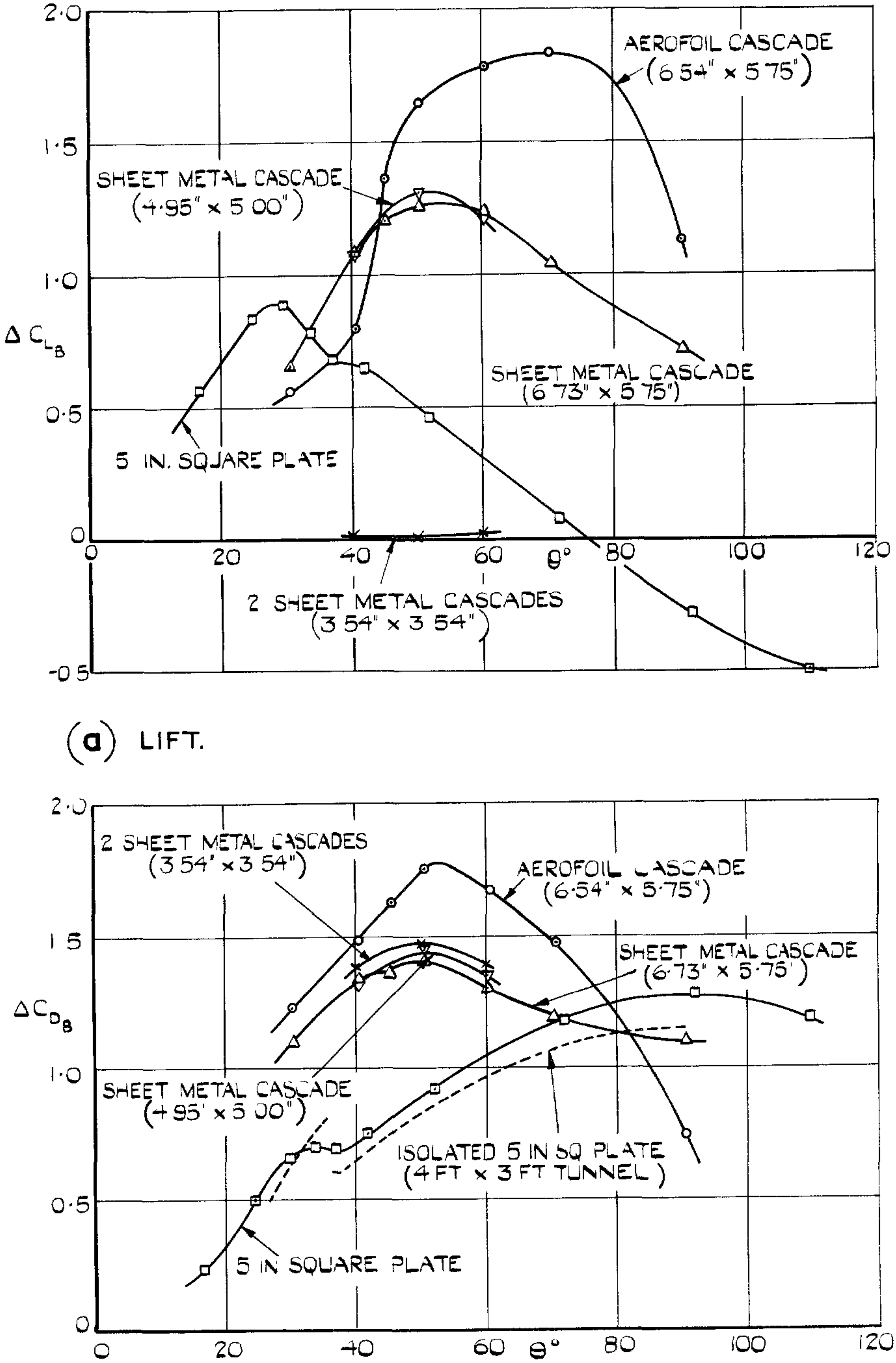

(a) LIFT.

(b) DRAG

NOTE COEFFICIENTS ARE BASED ON AREA REQUIRED TO STOW BRAKE

FIG. 19 (a & b) BRAKES ON 7 IN DIA BODY.

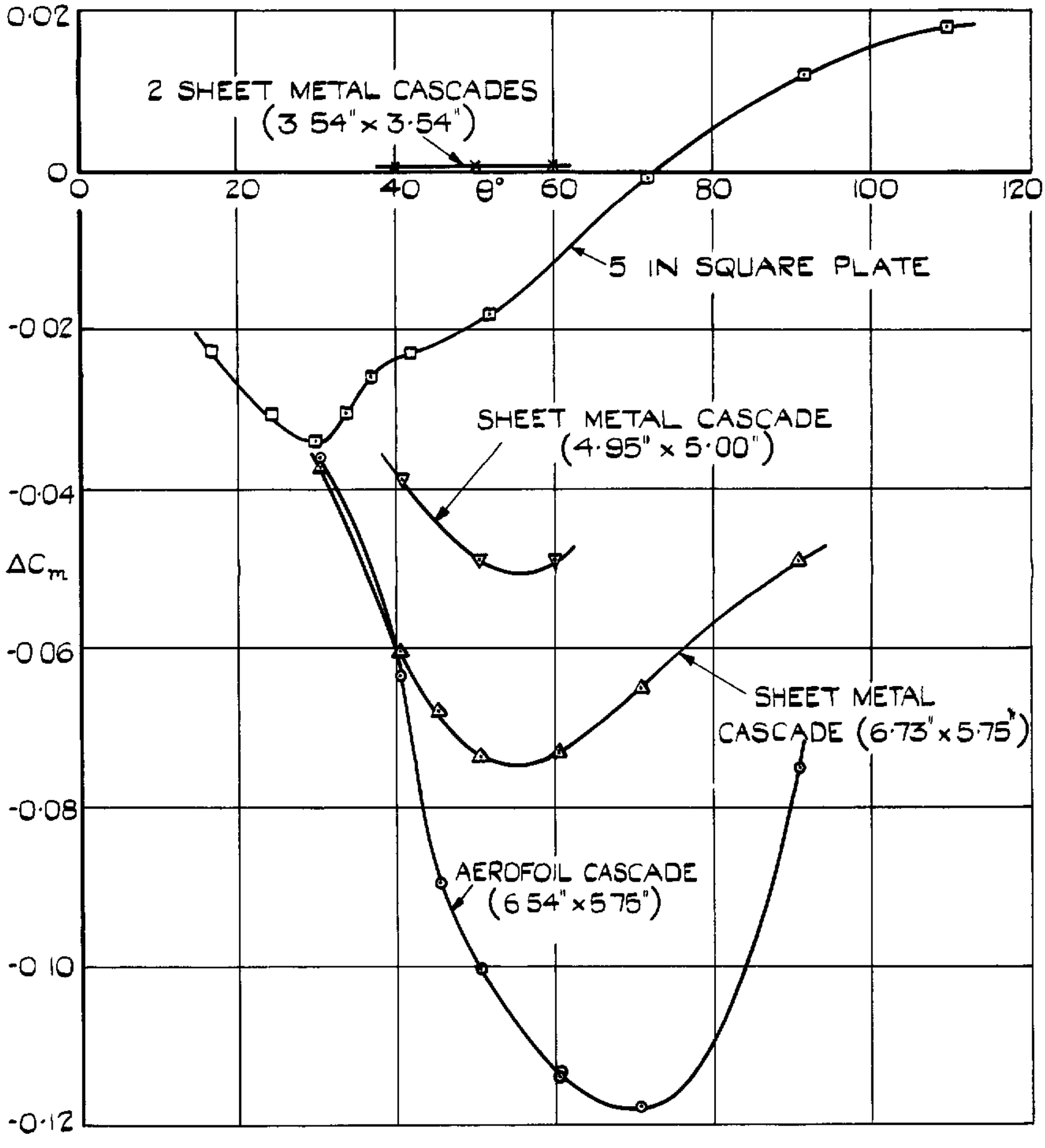

PITCHING MOMENT.

ΔC_m BASED ON HUNTER WING AREA (346 SQ FT) AND MEAN CHORD (10·33 FT) ASSUMING MODEL TO BE $\frac{1}{7 \cdot 5}$ SCALE

FIG. 20. BRAKES ON 7 IN DIA. BODY.

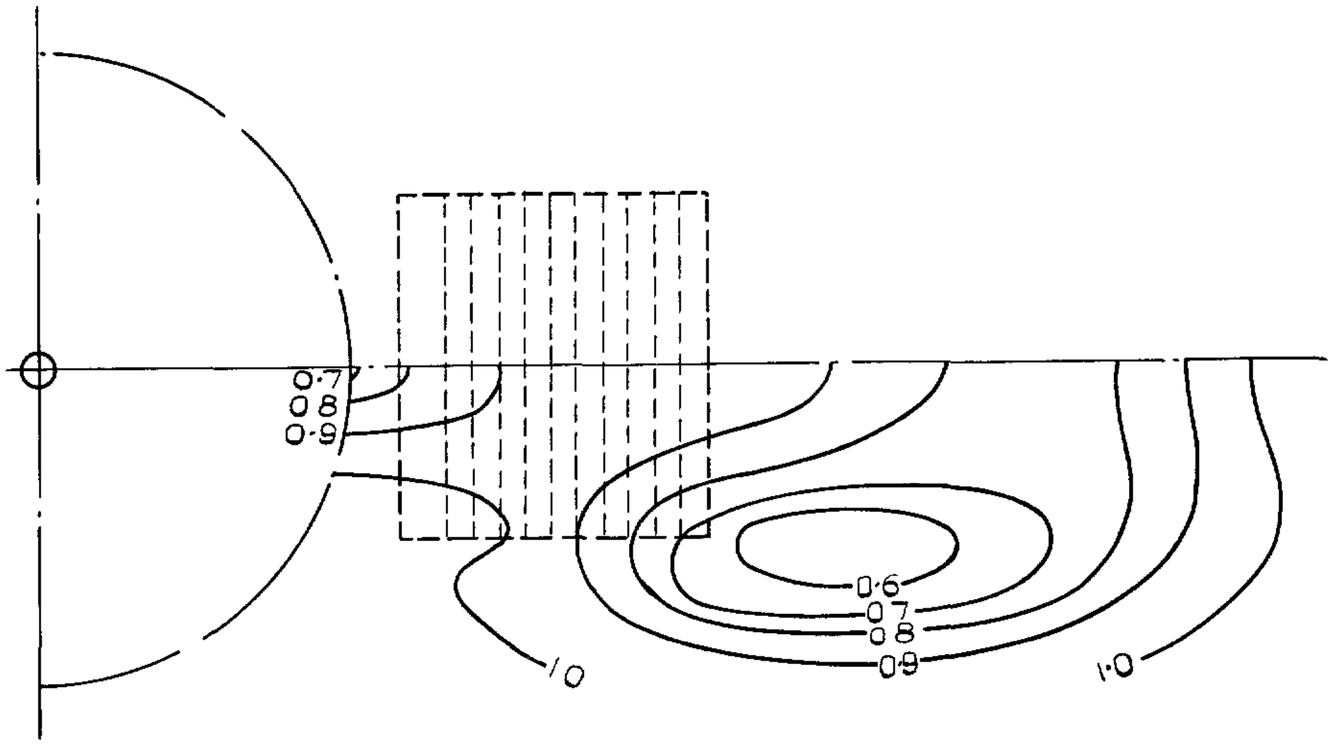

VELOCITY – CONTOURS OF $\frac{U}{U_o}$

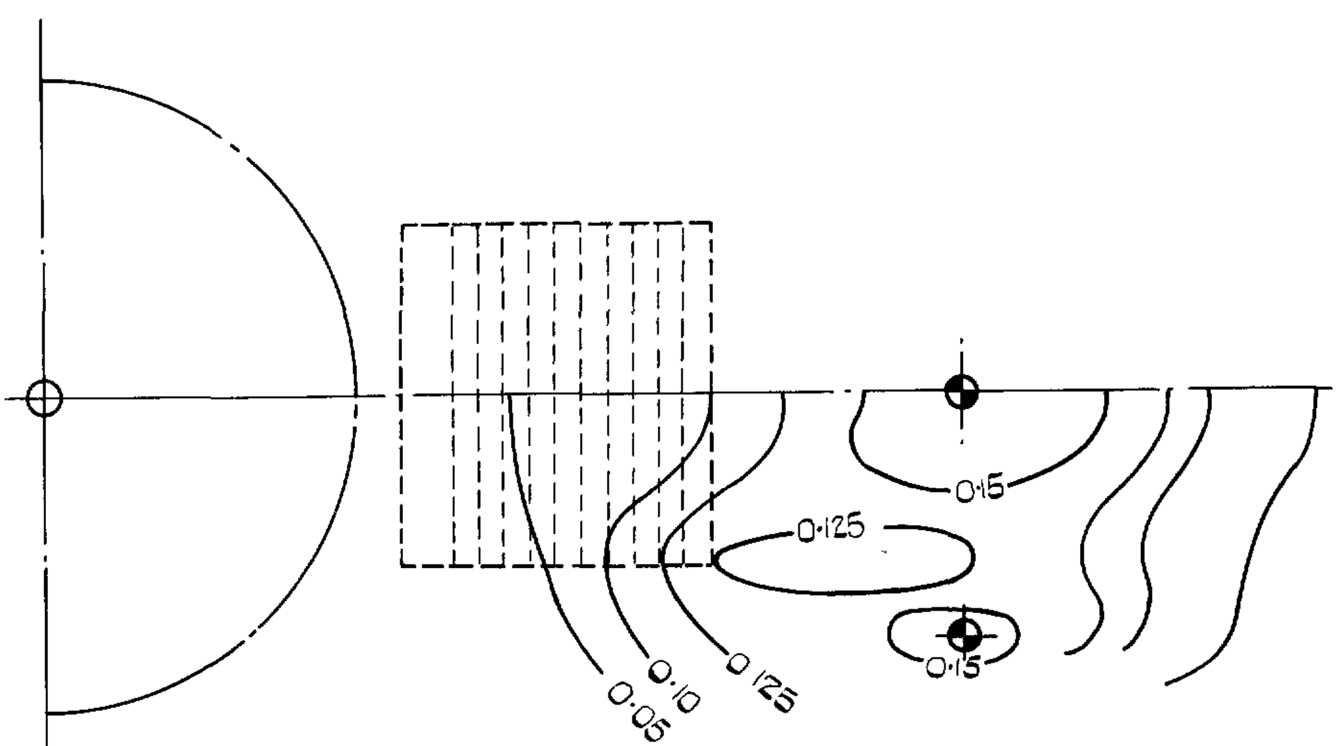

POINTS AT WHICH SPECTRA OF $\frac{u}{U_o}$ WERE MEASURED INDICATED THUS ⊕

VELOCITY FLUCTUATIONS – CONTOURS OF $\frac{u}{U_o}$

FIG. 21. FLOW BEHIND SHEET METAL CASCADE (3·54" X 3·54") ON 7 IN. DIA BODY.
MEASUREMENTS 15 IN DOWNSTREAM OF BRAKE HINGE
$\theta = 50°$

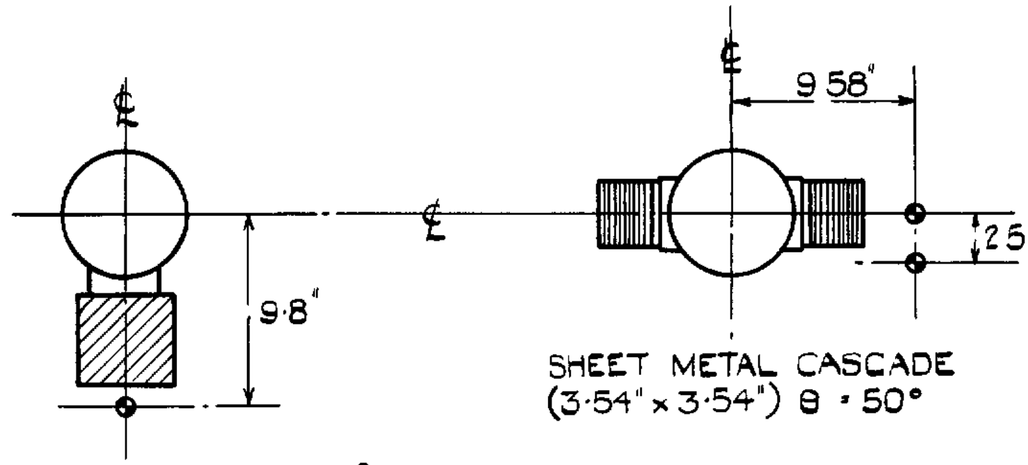

5 IN SQUARE PLATE θ·70°

SKETCHES SHOWING POINTS AT WHICH SPECTRA WERE MEASURED 15 IN BEHIND HINGE PLANE (FIG 18)

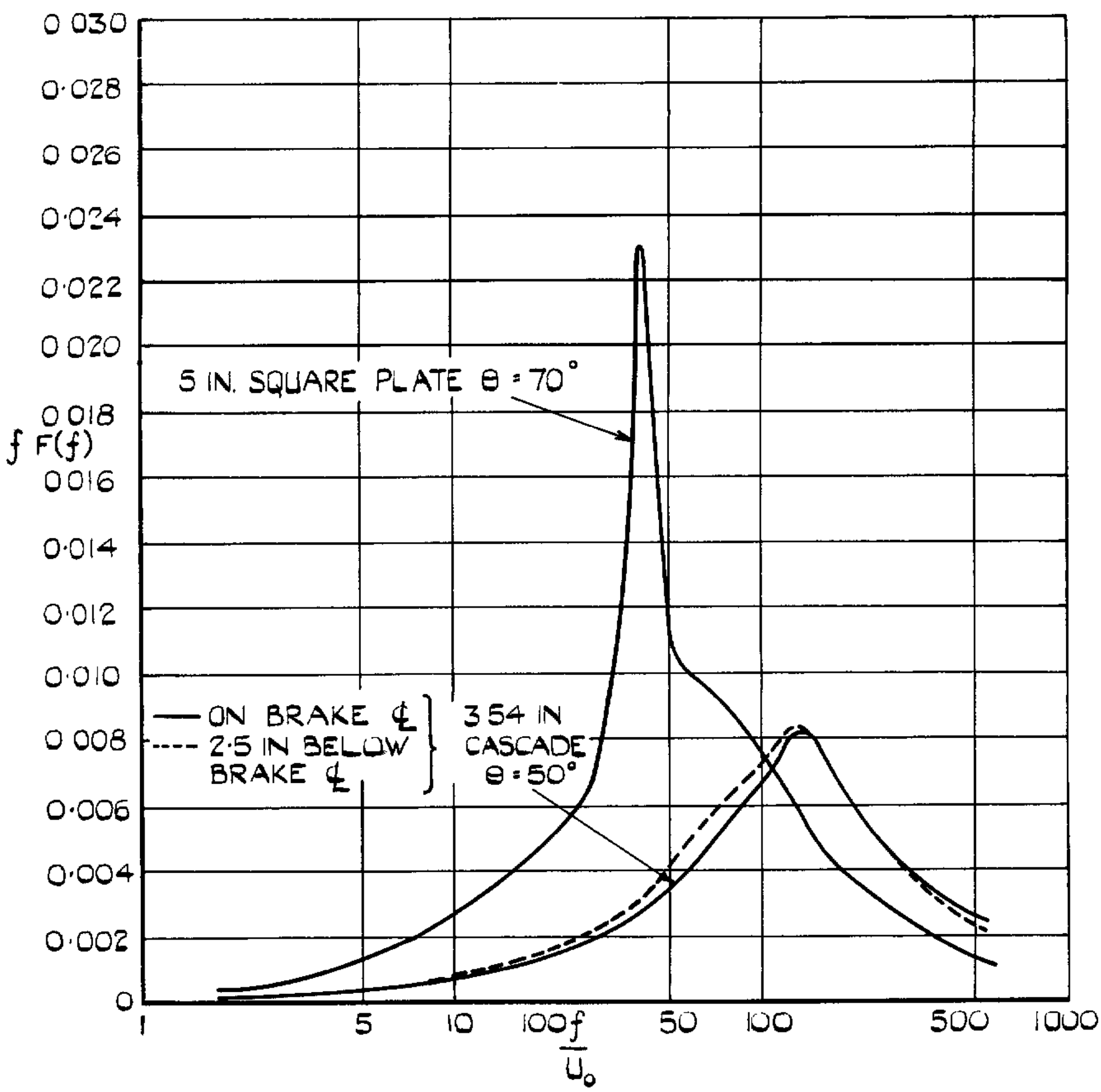

FIG. 22. FLOW BEHIND BRAKES ON 7 IN. DIA. BODY SPECTRA OF $\frac{u}{U_o}$

C.P. No. 251
(17,566)
A.R.C. Technical Report

Crown copyright reserved

Published by
HER MAJESTY'S STATIONERY OFFICE
To be purchased from
York House, Kingsway, London W.C.2
423 Oxford Street, London W.1
P.O. Box 569, London S.E.1
13A Castle Street, Edinburgh 2
109 St. Mary Street, Cardiff
39 King Street, Manchester 2
Tower Lane, Bristol 1
2 Edmund Street, Birmingham 3
80 Chichester Street, Belfast
or through any bookseller

PRINTED IN GREAT BRITAIN

S.O. Code No. 23-9009-51

Wt.2078.K3

C.P. No. 251